Dissolution Anisotropy of Pyroxenes: Role of Edges and Corners Inferred from Stochastic Simulations of Enstatite Dissolution

Arnaud Bouissonnié, Damien Daval, Philippe Ackerer

THE JOURNAL OF PHYSICAL CHEMISTRY C
A JOURNAL OF THE AMERICAN CHEMICAL SOCIETY

pubs.acs.org/JPCC Article

Dissolution Anisotropy of Pyroxenes: Role of Edges and Corners Inferred from Stochastic Simulations of Enstatite Dissolution

Arnaud Bouissonnié,* Damien Daval, and Philippe Ackerer

Cite This: https://doi.org/10.1021/acs.jpcc.0c11416 Read Online

ABSTRACT: Experimental studies exhibit a wide variety of dissolution rates for a given mineral depending on the chemical conditions and also on the type of experiment conducted. As a relevant example, studies focused on face-specific dissolution and those focused on powder dissolution can present differences of up to 1 order of magnitude. Linking these two types of experiments is therefore relevant, since experimental conditions can be almost entirely controlled throughout the entire experiment. In this study, we use a stochastic dissolution model based on hydrolysis of atomic bonds of enstatite, the magnesium endmember pyroxene, to simulate the dissolution of different sizes and aspect ratios of enstatite grains. This model, validated in a previous study by a comparison with experimental (face-specific) rate data, is used to understand the evolution of the dissolution rate with time, from the beginning of the dissolution until the entire consumption of the crystal. We show that the behavior of the dissolution is controlled mainly by the aspect ratio of the grain. A simple dissolution model based on face-specific dissolution is then used to compare the results of the simulations obtained with those resulting from the grain dissolution model. The similarity between the results points out that the contribution to the dissolution of edges and corners is only modest for very anisotropic silicates such as pyroxenes, where silicate tetrahedrons are connected through chains running parallel to a given crystallographic axis. This simple model is then extended using both face-specific experimental and model results and compared to existing powder dissolution results. This comparison shows an excellent agreement between face-specific dissolution modeling and powder dissolution experiment, indicating that, for anisotropic minerals such as pyroxenes, face-specific and powder dissolution experiments can be linked, which can be of great interest for future dissolution studies.

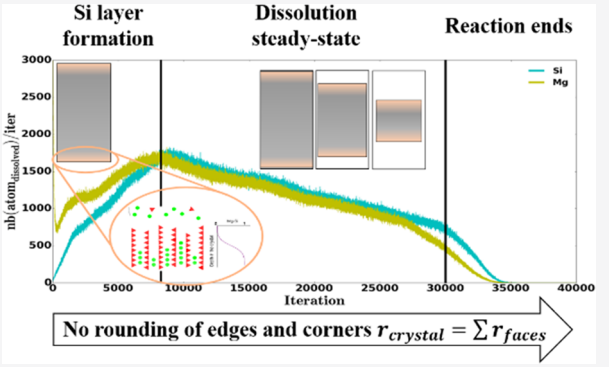

1. INTRODUCTION

Dissolution kinetics is a key parameter to understand the Earth's surface evolution and is crucial for several industrial and environmental problems (cement dissolution, nutrient depletion in soils, etc.). Over the last decades, numerous studies have helped understand the processes that occur at the mineral–water interface, as well as developing different methods to measure their kinetics for a wide variety of minerals.[1−9] While most of these studies are based on powder dissolution experiments,[2,10−12] fewer studies succeeded to measure dissolution rates on different faces of a given mineral.[3,4,6,7,9,13−16] This latter kind of studies has shown the importance of the crystallographic structure (i.e., anisotropy) on mineral dissolution kinetics. As a relevant example, pyroxenes, which are strongly anisotropic due to their silica tetrahedron chains, exhibit a strong dissolution anisotropy consistent with the periodic bond chain theory.[17] However, the comparison between the dissolution rates measured on single faces and those measured on powder highlights a significant difference (powder dissolution rates are generally higher than face-specific dissolution rates[18]). This adds complexity to our ability to upscale dissolution rates and to apply experimental measurements on field studies without using empirical scaling parameters that complicate reactive-transport simulations.

As suggested by different studies, this difference may result from the amount of reactive sites present in each case.[19−23] Indeed, considering face dissolution often means considering a reactive surface which is not affected by the dissolution of mineral's edges and corner. However, not only these sites are the most reactive, as shown in Noiriel et al.,[24,25] they are also present in greater proportions in powders than on centimeter-sized single crystals (if one assumes a flat surface at the beginning of the experiments). Therefore, studying the contribution of these corners and edges to dissolution is essential. To do so, new

Received: December 23, 2020
Revised: March 27, 2021

https://doi.org/10.1021/acs.jpcc.0c11416
J. Phys. Chem. C XXXX, XXX, XXX−XXX

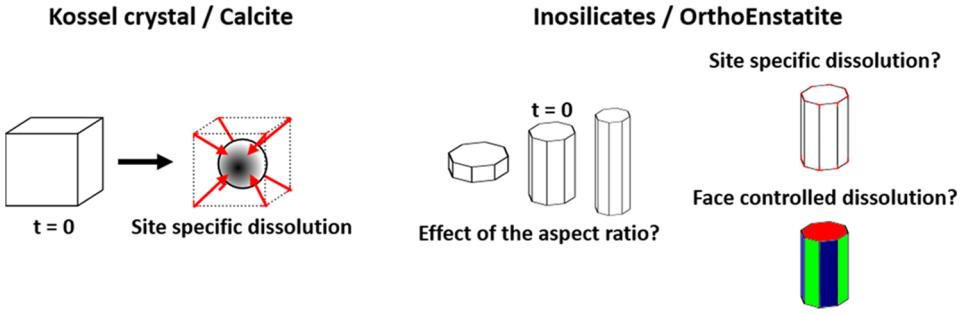

Figure 1. Schematic representation of the objectives of this paper. Dissolution is often assumed to take place on reactive sites such as edges and corners. It has been demonstrated on Kossel crystal and calcite that, during the dissolution process, the shape of the crystal evolves, and edges and corners are rounded, leading to an almost spherical shape (for Kossel crystal, depending on the activation energy of the hydrolysis) when the primal material is a cube. In this study, we aim to determine whether these considerations are applicable on inosilicates, with a specific focus on enstatite. The study is based on simulations using a stochastic dissolution model applied at the atomic bond level and aims to explore different aspect ratios of the initial mineral parallelepipedal shape.

experimental setups have emerged, using analytical techniques such as X-ray tomography[24−26] or vertical scanning interferometry.[27] However, despite their increasing efficiency to study the processes that occur at finer scales (micrometer to nanometer scale), they often need to be combined with numerical studies to unravel what happens at the solid−fluid interface.

Numerical experiments have become a powerful tool to improve our understanding of processes occurring at the water−mineral interface, ranging from molecular dynamics to reactive-transport model used at pore scale.[28−30] The last decades have also seen the development of stochastic dissolution models, such as kinetics Monte Carlo models or Voronoï method.[13,19,23,31−38] These models, based on a relation between the activation energies of individual processes (bond hydrolysis, for example) and their occurrence probability, allow for fast computation and the simulation of larger objects, which classical molecular dynamics is not able to deal with. These models, first applied on Kossel crystals, have brought or validated many important results. As an example, numerous studies applied on Kossel crystals validate the difference of reactivity between the crystal's edges, corners, and surfaces.[19] The work of Zhang and Luttge[35] also mentioned these differences for feldspar dissolution. However, providing a generalization to other minerals, which is an intrinsic issue belonging to the field of physical chemistry, is important and may present a great interest to link laboratory and field observations, as mentioned by Noiriel et al.[25]

For several reasons, pyroxenes represent a relevant target to address these aspects. Indeed, not only do they have a strongly anisotropic structure (silica chains running parallel to a given crystallographic axis), but they are also present worldwide and represent a major group of minerals for reactive-transport models.[39,40] In two previous studies,[16,41] we described a stochastic dissolution model operating at atomic scale and applied to enstatite, the magnesian endmember of pyroxenes. This model, validated by a comparison between simulations and experimental results, has shown its ability to reproduce the dissolution anisotropy of enstatite as well as the surface features observed at the end of the experiments (etch pit morphology, and relative thickness of the silica layers developed on each face).[16] However, in these two studies, we focused on face-specific dissolution, neglecting the contribution of "macro-corners" and "macro-edges", which can represent, for some minerals such as calcite, the most reactive sites.[25] In the present study, we propose to simulate the dissolution of enstatite rectangular parallelepipeds. Different sizes and aspect ratios are modeled and analyzed, to understand if the dissolution of enstatite grains can be described mathematically using parameters related to the grain dimensions, as well as to understand if observations made on calcite[25] are expandable to enstatite, and more generally, to pyroxenes. Another objective deals with the impact of the aspect ratio of a grain on the dissolution rate. Powder experiments present a wide variety of grain morphologies resulting from the crushing of macro-crystals. These different shapes and sizes may affect the dissolution rate, since the dissolution rate is face-specific.[3,15,16] Furthermore, different grain sizes may imply a greater rate variability through the development of fast dissolving micro-facets at mineral's edges and corners. These questions are summarized in Figure 1.

2. METHODS

2.1. Model Description. A complete description of the model is given in Bouissonnié et al.[16] Briefly, atoms contained in the enstatite cell are placed using *Pbca* space group symmetry elements, using the cell parameters (a = 18.233 Å, b = 8.8191 Å, and c = 5.1802 Å) and the coordinates given by Hugh-Jones and Angel.[42] Each magnesium and silicon atom is linked to oxygen according to their coordination. However, the dissolution of oxygen atoms is never considered in the dissolution model. Indeed, they are considered as bridging atoms[13] and the dissolution model is applied on M−O_{br}−M bonds (M being a Mg or Si atom). All atoms linked to another one via a bridging oxygen are part of its first coordination sphere.[13] Only the first coordination sphere is taken into account to compute the bond-breaking probabilities, since previous results showed that this strategy results in a satisfactory agreement between modeled and experimental results.[16]

Usually, the probability attributed with one event (i.e., the bond-breaking probability) is written as follows[38]

$$P = e^{-E_a/k_B T} \quad (1)$$

where P stands for the bond-breaking probability, E_a is the activation energy of the bond hydrolysis (J), k_B is the Boltzmann constant (J/K), and T is the temperature (K). In the present study, the greatest bond-breaking probability (i.e., the bond hydrolysis associated with the lowest activation energy, Mg−O−Mg) was arbitrarily set to 0.99 and the two other probabilities were scaled according to the differences between their corresponding activation energies following

https://doi.org/10.1021/acs.jpcc.0c11416
J. Phys. Chem. C XXXX, XXX, XXX−XXX

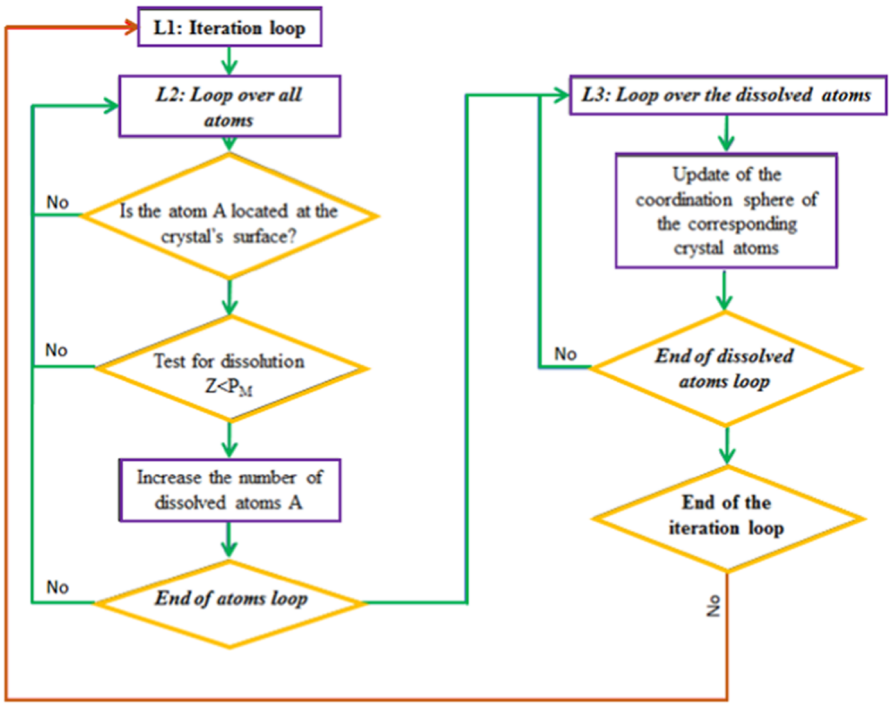

Figure 2. Scheme of the dissolution algorithm used in the dissolution model. This scheme is adapted from Bouissonnié et al.[41]

$$\frac{P_A}{P_B} = e^{-(E_a^A - E_a^B)/k_B T} \quad (2)$$

where A and B represent two different bonds. According to the best agreement between modeled and experimental results developed in Bouissonnié et al.,[16] the other two probabilities were calculated as 0.4 and 0.0146 for Mg−O−Si and Si−O−Si, respectively. The probability of backward reactions (i.e., the creation of a new bond, previously destroyed or not) is not considered here since the model is applied to reproduce experiments run at pH 0,[16] where these reactions can be neglected.

As it has been shown to successfully reproduce experimental data and observations, an "all-or-none" approach was used in this study.[13,19,35−37,43,44] This approach considers that an atom is released only if all bonds that connect it to the surface are simultaneously broken during a single iteration step. Hence, the numerical model works directly on the atoms, and not on the bonds. Then, the overall probability of an atom to be released into solution during one iteration is given by the product of all of the probabilities corresponding to the different bonds it shares with other atoms

$$P_M = e^{-nE_{M-O-Mg}/k_B T} e^{-mE_{M-O-Si}/k_B T} = P_{M-O-Mg}^n P_{M-O-Si}^m \quad (3)$$

where n and m stand for the number of bonds that the considered atom shares with neighboring Mg and Si atoms, respectively.

2.2. Dissolution Algorithm. At each iteration step, all atoms located at the surface are scanned. An atom is considered at the surface if its first coordination sphere is incomplete. A random number Z is generated for each atom; if $Z < P_M$, the atom is released into the solution, if not, the scan of the atoms moves on. At the end of the iteration, i.e., after scanning all atoms located at the surface, the attributes of the atoms contained in the first coordination sphere of those which have been dissolved during the iteration, are updated to consider this change, resulting in an increase of their departure probability at the next iteration. It is essential to update the attributes of the considered atoms only at the end of an iteration to avoid an "in cascade" dissolution, where the atoms would be released one after the other due to a direct change of the probabilities. A scheme of the algorithm is shown in Figure 2.

2.3. Output of the Model. The dissolution was monitored based on the release of Si atoms, as in classical studies dedicated to silicate dissolution kinetics. Note that because the dissolution at steady state (i.e., the dissolution rate can be considered to be constant) is stoichiometric,[16] this choice has no consequence on what will be described in the present study. However, the behavior of Mg release is important at the beginning of the dissolution process[16] and will be discussed in the section corresponding to this part of the dissolution timeline.

In the literature, the term "mineral dissolution rate" is usually used to refer to the release rate of atoms in the solution from a mineral surface, whether or not it is normalized to the contact surface between the fluid and the mineral. To avoid any confusion, in the following, we will use the term "dissolution rate" to refer to a velocity that is not normalized to the surface area (unit: mol/iteration) and "dissolution flux" to refer to dissolution rates normalized with respect to the surface area (unit: mol/m^2/iteration). Both quantities are calculated at each iteration for any numerical simulation.

The cumulated number of released atoms has been used to calculate the total surface retreat during the simulations corresponding to the dissolution of single faces (i.e., only one face is considered to be in contact with the solution). The surface retreat is defined as the average height of material lost during the dissolution. It is calculated as follows

$$\Delta h_i^{(hkl)} = \frac{a^* b^* c}{16^* S_f} \sum_i^{n=1} n b(Si_{d,n}) \quad (4)$$

https://doi.org/10.1021/acs.jpcc.0c11416
J. Phys. Chem. C XXXX, XXX, XXX−XXX

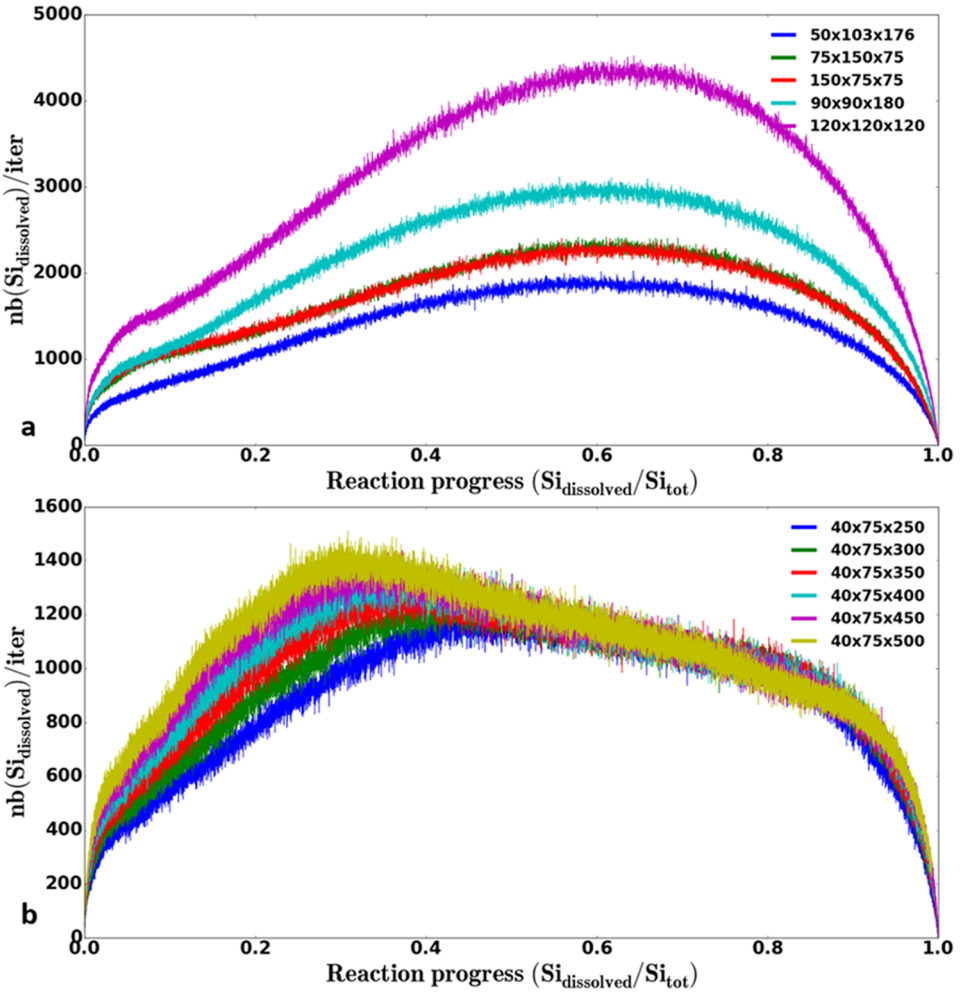

Figure 3. Results of the dissolution model showing the dissolution rate (defined as the number of Si atoms released per iteration) as a function of the reaction progress. Legends indicate how many times the crystal cell is multiplied in *x*, *y*, and *z* directions. The results reported here represent sets of simulations applied on arbitrary parallelepiped sizes (i.e., not representative of the aspect ratio of natural enstatite). (a) First subgroup of simulations, with arbitrary rectangular parallelepiped dimensions. (b) Second subgroup: Length and width (parallel to the *a* and *b* axes of the enstatite cell) of the rectangular parallelepiped were kept constant while the height (parallel to the *c* axis) was modified in the different simulations. In both cases, a similar behavior is observed. (a) Simulations highlight a parabolic behavior of the dissolution. The maximum seems to be observed at similar values of the reaction progress. (b) Contrary to the first set, the simulations of the second set are different at the beginning of the dissolution. Here, the larger the crystal, the higher the maximum. After reaching the maximum, the number of Si atoms dissolved decreases linearly. The slope is the same for each simulation.

where $\Delta h_i^{(hkl)}$ is the surface retreat at the *i*th iteration (m); *a*, *b*, and *c* are the cell parameters (m); S_f is the surface area of the face (m^2); and $nb(Si_{d,i})$ is the number of Si atoms dissolved at the *i*th iteration. The number 16 corresponds to the number of Si atoms in the enstatite cell. This method has been validated in Bouissonnié et al.[16] and gives identical results to those obtained if the mean coordinates in the direction normal to the surface were used.

Finally, the last parameter used in this study is the advancement of the dissolution reaction. It is defined as the ratio between the number of Si atoms dissolved from the beginning of the simulation and the initial number of Si atoms at the beginning of the simulation.

2.4. Assumptions and Limitations of the Model. The model has proven its ability to reproduce both experimental dissolution rates and observed surface features evolutions. However, several assumptions (all based on the studied chemical condition) are considered and may impact the model outputs and their upscaling to study natural environment:

- No backward reactions (i.e., formation of atomic bonds) are implemented. This simplification was made because of the very low pH of the studied solution (pH 0). This pH makes the solution to be very far from the thermodynamic equilibrium with respect to enstatite. Therefore, backward reactions (i.e., formation of atomic bonds) are considered unlikely to happen.
- The dissolution algorithm is applied on atoms rather than atomic bonds. This method is commonly used in stochastic dissolution studies, however, combined with the first assumption, this precludes the formation of amorphous silica layers resulting from interfacial dissolution−reprecipitation[45] or reorganization of dangling bonds.[46] In the present study, such layers are suspected to have no impact on the dissolution rate because their passivating ability is thought to be pH-dependent[14,47] and passivating layers are unlikely to form in strongly acidic environments. Such conditions may limit the extension of the conclusions of the study to less acidic environments.

https://doi.org/10.1021/acs.jpcc.0c11416
J. Phys. Chem. C XXXX, XXX, XXX−XXX

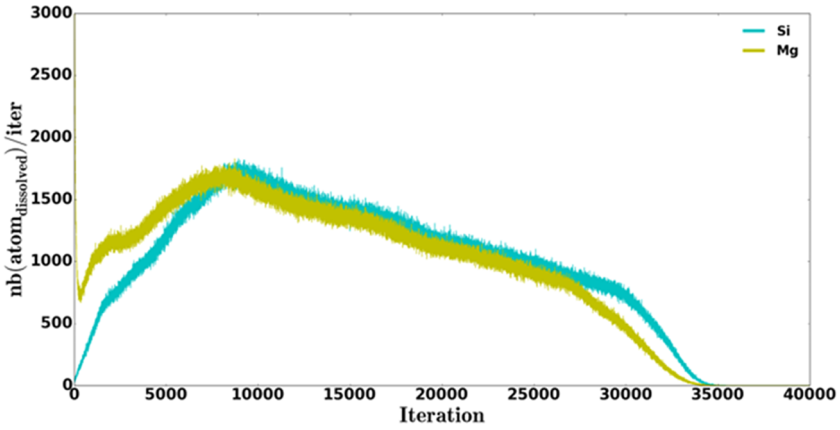

Figure 4. Example of the results of a simulation conducted on a 40a × 82b × 700c volume. This figure shows the dissolution rate (number of dissolved atoms per iteration) as a function of the number of iteration steps. The cyan curve represents Si atoms, and the dark yellow curve represents Mg atoms. Contrary to the Si curve, which increases continuously at the beginning of the simulation, the Mg curve is marked by a sharp decrease of the number of atoms released per iteration. This is explained by the fast depletion of superficial Mg, which have a high probability of departure. After reaching the maximum value of the amount of Si and Mg released per iteration (corresponding to the iteration where the silica layer reaches a constant thickness), the dissolution rate decreases continuously and the dissolution is stoichiometric.

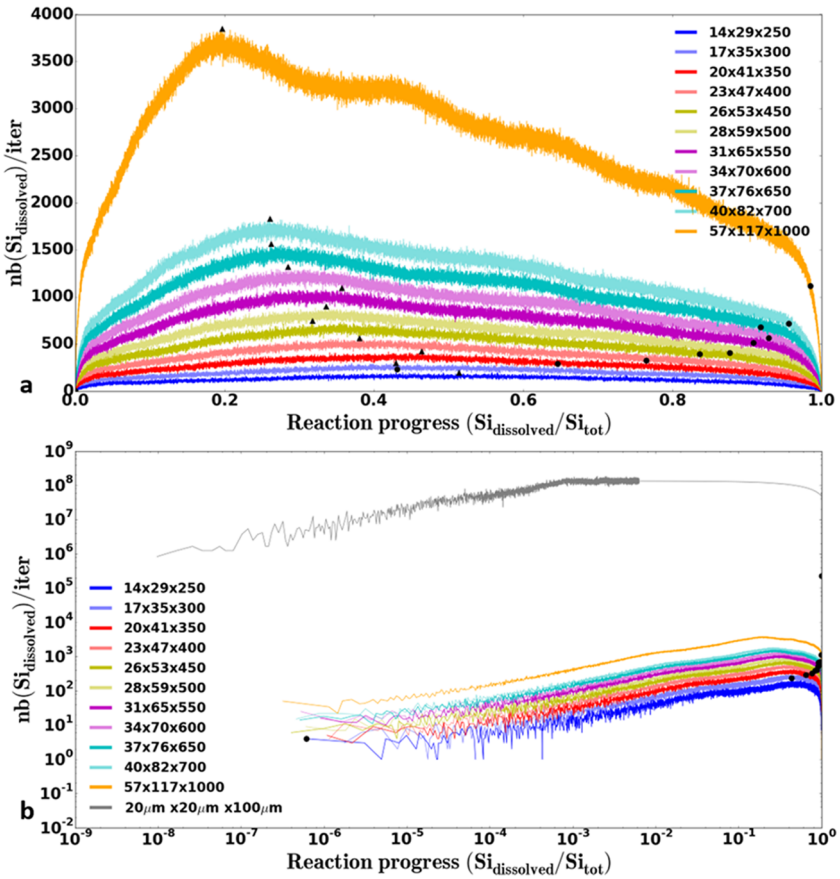

Figure 5. (a, b) Results of the dissolution model showing the dissolution rate (defined as the number of Si atoms released per iteration) as a function of the reaction progress. Legends indicate how many times the crystal cell is multiplied in *x*, *y*, and *z* directions or exact dimension (black line). Each panel represents Si dissolution rate as a function of the reaction progress for the set of simulations that observe realistic aspect ratios for the grains, plotted in standard and logarithmic scales, respectively. Black triangles indicate the reaction progress where the dissolution rate reaches its maximum. Black circles indicate the reaction progress where the volume of the enstatite grain is equivalent to that of the initial smallest simulated rectangular parallelepiped (14 × 29 × 250). For each simulation, the dissolution rate increases at the beginning of the process, until reaching Aconitum maximum value. After the maximum value is reached, the dissolution rate decreases linearly until the reaction progress reaches ~95%. The duration of the linear decreasing phase depends on the crystal size: the larger the crystal, the longer the linear phase.

However, the conclusions reached in the present study may remain valid even in conditions where the fluid is less acidic, as long as the fluid is at far from equilibrium with respect to $SiO_{2(am)}$, since presumptive passivating layers

https://doi.org/10.1021/acs.jpcc.0c11416
J. Phys. Chem. C XXXX, XXX, XXX−XXX

would be unstable and therefore, would not be rate-controlling of the dissolution process.[48]

- The simulations correspond to conditions where the aqueous solution is continuously stirred, resulting in no local variations of the saturation index of the solution. Therefore, the saturation index is supposed to be constant (and far from equilibrium), both in space and time.

3. RESULTS

3.1. Evolution of Si Dissolution. A total of 22 different enstatite volumes have been simulated. In the following, each volume is named after the number of cells in the three spatial directions.

The first 11 simulations were conducted using arbitrary volumes to highlight potential similarities between their dissolution behaviors. The results of these simulations are given in Figure 3. This group of simulations can be separated into two main subgroups (Figure 3a,b). The first subgroup (Figure 3a) presents results of simulation runs with initial aspect ratios that have no particular relation to each other, unlike the second subgroup (Figure 3b), which contains simulations made on grains varying only in height (the length in the x and y directions having been kept constant).

The first subgroup is marked by a sharp increase of the amount of dissolved Si atoms within the first 3−5% of the reaction, which corresponds to an increase from 0 to 500−1400 Si atoms released into solution per iteration, depending on the initial volume. After this first step, the behavior of the release rate of Si differs from the simulated volume. Indeed, while smaller volumes ($50 \times 103 \times 176$, $75 \times 150 \times 75$ and $150 \times 75 \times 75$) are characterized by a linear increase extending over almost 40% of the reaction, the others ($90 \times 90 \times 180$ and $120 \times 120 \times 120$) show a shorter linear evolution (only 20% of the total reaction). In each case, after the linear increase of the release rate of Si into solution, a slower increase is observed until the dissolution rate reaches its maximum, which occurs after a similar reaction progress (between 60 and 65%) for all volumes of this subgroup. The dissolution rate reaches ∼1900, 2300, 2300, 2950, and 4350 Si atoms/iteration for the $50 \times 103 \times 176$, $75 \times 150 \times 75$, $150 \times 75 \times 75$, $90 \times 90 \times 180$, and $120 \times 120 \times 120$ volumes, respectively. After this maximum is reached, the dissolution rate of Si decreases until the reaction is complete, and all of the crystal has been dissolved. This step extends over the last 35−40% of the total reaction.

The second subgroup of simulations is composed of six different volumes. While these volumes differ in height (length in the z direction parallel to the c axis), the lengths in the x and y directions were kept constant. Hence, the surface area of (100) and (010) faces varied, unlike that of the (001) faces. The onset of the simulations exhibits a similar behavior to that described for the first subgroup: the first 3% of the reaction is characterized by a sharp increase (from 0 to 350−600 Si atoms/iteration) of the release rate of Si. This step is followed by a linear increase of the dissolution rate until it reaches its maximum. Contrary to the first subgroup of simulations, the advancement corresponding to this maximum depends on the size of the initial volume. Indeed, if the maximal dissolution rate is greater for the largest volume (1390 Si atoms/iteration for the volume $40 \times 75 \times 500$) compared to the smallest one (1190 Si atoms/iteration for the volume $40 \times 75 \times 250$), the advancement at which the maximum is reached is lower (0.30 against 0.45, respectively). Another difference between the first and second subgroups is the behavior of the dissolution after the maximum is reached. While, in the first case, the dissolution rate decreases sharply until the end of the reaction, in the second case, a slow and linear decrease is observed from an advancement of 30−45 to 85−90% depending on the considered volume. During this linear decrease, regardless of the volume, all simulation results are almost identical, showing the same dissolution rate of Si atoms at the same advancement of reaction. The last 10−15% of the reaction is characterized by a sharp decrease of the dissolution rate of Si atoms to finally reach 0 when the reaction is complete (Figure 4).

The second group of eleven simulations is shown in Figure 5. Contrary to the previous group of simulations, the aspect ratios which were used are representative of natural enstatite crystal habit. In spite of these differences, the evolution of the dissolution rate of Si atoms is almost identical to that described for the second subgroup of the first group described above, with the following steps: (1) a sharp increase of the Si dissolution rate during the first 3% of the dissolution, (2) a linear increase until the maximum is reached (from 145 to 3660 Si atoms released per iteration, reached after a reaction progress of 40−20% for the smallest and the largest volumes, respectively), (3) a linear decrease in the release rate of Si until 90−95% of the reaction, and finally (4) a sharp decrease in the release rate of Si over the last 5−10% of the reaction.

3.2. Evolution of Mg Dissolution. The behavior of Mg dissolution is similar to the one described above for Si dissolution (Figure 4). The main differences are observed at the very beginning and at the end of the simulations. Mg dissolution evolution has been studied only for simulated volumes representative of natural aspect ratios of enstatite. Because all simulations, as for Si atoms, exhibit a similar behavior, only one case is shown in Figure 4 ($40 \times 82 \times 700$). The global trend of Mg dissolution evolution is as follows:

- A dramatic decrease of the dissolution rate at the beginning of the reaction (325 iterations for the volume shown in Figure 4).
- An increase of the dissolution rate from the 315th to the 8000th iterations. This increase is marked by two pulses for the volume presented in Figure 4.
- A linear, slow decrease of the dissolution rate, similar to the one observed in the case of Si dissolution. In the $40 \times 82 \times 700$ volume, this step extends from the 8000th to the 26 990th iterations.
- A more pronounced decrease in the dissolution rate for the last iterations until all of the Mg atoms have been dissolved.

3.3. Dissolution Normalized Per Surface Unit. Because the most realistic cases treated in this study are those that observe the aspect ratio of pyroxenes, only the corresponding simulations were investigated with respect to a normalization per surface unit. The evolution of the surface area is not derived from direct outputs of the simulations. Instead, it is assumed that the surface decreases according to the retreat of each single face of the simulated volumes. In Bouissonnié et al.,[16] we investigated the surface retreat of (100), (010), and (001) faces, demonstrating that our model was able to reproduce observed experimental data. Similar simulations were then used to calculate the evolution of the surface area of the simulated crystals according to the following equation

https://doi.org/10.1021/acs.jpcc.0c11416
J. Phys. Chem. C XXXX, XXX, XXX−XXX

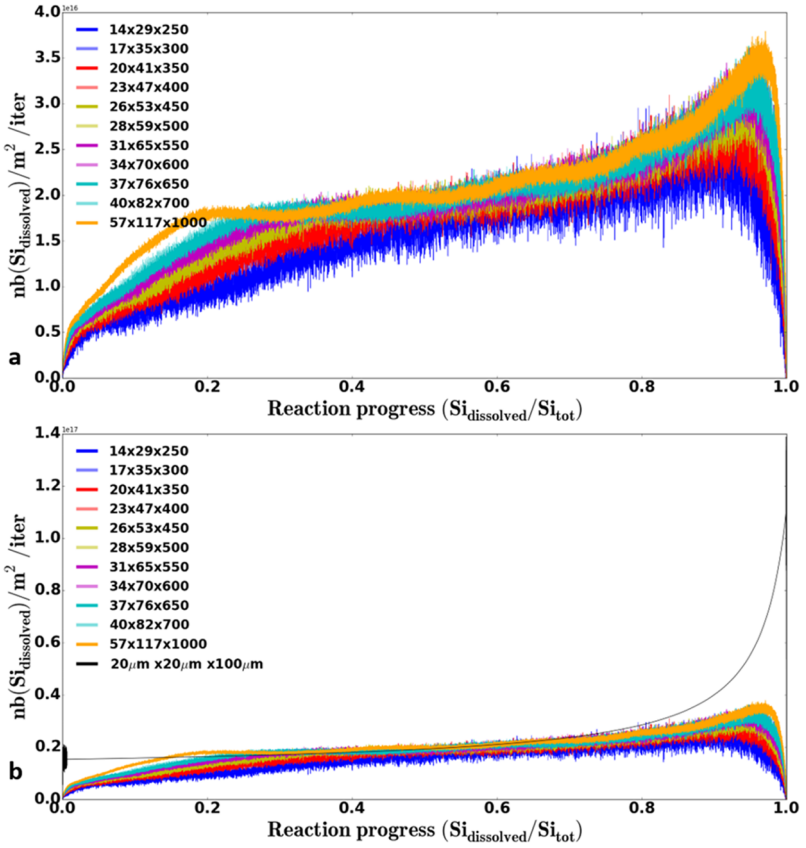

Figure 6. Dissolution flux as a function of the reaction progress. Legends indicate how many times the crystal cell is multiplied in the *x*, *y*, and *z* directions. (a) Results of the simulations. (b) Results of the simulations and modeled theoretical result for enstatite grain with realistic grain size (black curve). The black patch at the beginning of the realistic grain size dissolution corresponds to the stages 1 and 2 of Figure 9a,b. In each case, the dissolution flux increases at the beginning of the simulations. After reaching a given value of the reaction progress (corresponding to the 8000th iteration), the increase slows down and the dissolution flux can be considered as constant for few iterations (the larger the crystal, the longer the "steady-state" regime). Then, a moderate increase is observed until the dissolution reaches its maximum. After reaching its maximum, the dissolution flux decreases dramatically and reaches zero when all of the atoms have been dissolved.

$$A(i) = 2[(x_0 - 2\Delta h_i^{(100)})(y_0 - 2\Delta h_i^{(010)}) + (y_0 - 2\Delta h_i^{(010)})(z_0 - 2\Delta h_i^{(001)}) + (x_0 - 2\Delta h_i^{(100)})(z_0 - 2\Delta h_i^{(001)})] \quad (5)$$

where $A(i)$ is the surface area at the ith iteration; x_0, y_0, and z_0 are the initial lengths in the *x*, *y*, and *z* directions, respectively; and $\Delta h_i^{(hkl)}$ is the surface retreat of the corresponding (hkl) face at the ith iteration, derived from the simulations performed on single faces where the edges were constrained to be nonreactive. This method, however, does not take into account a possible rounding of the edges, often observed in mineral dissolution experiments and modeling.[23,25,49] The number of Si atoms released at each iteration is then divided by the surface area at the corresponding iteration.

Results are shown in Figure 6. The trends followed by the dissolution fluxes differ from those obtained for dissolution rates. The first 3.5−1% of reaction is characterized by a sharp increase in the dissolution flux from 0 to 5.4−6.2 × 10^{15} Si atoms/(m^2 iteration) for the smallest and largest volumes, respectively. The increase in the dissolution flux is then less pronounced over the next 42.5−19% of the reaction. The Si dissolution flux reaches 1.6 × 10^{16} Si atoms/(m^2 iteration) at 47% of the reaction progress for the smallest volume against 1.8 × 10^{16} Si atoms/(m^2 iteration) at 20% for the largest one. After this period, the dissolution flux tends to stabilize for the three largest volumes but only over a short reaction progress (approximately 10% of the total reaction). After this phase, the dissolution flux of the largest volumes follows that of the smallest ones. The dissolution flux still increases, but the difference between each iteration is less pronounced until the reaction progress reaches 90−96% (where the dissolution flux reaches its maximum: (2.2−3.5) × 10^{16} Si atoms/(m^2 iteration) for the smallest and largest volumes, respectively). Finally, from 90 to 96% of the dissolution, the Si dissolution flux decreases sharply to reach 0 when the volume has been completely consumed.

4. DISCUSSION

4.1. Evolution of Mg and Si Dissolution Rates.

4.1.1. Evolution during the First 8000 Iterations. Despite the differences in volumes used in the simulations, all simulation outputs are characterized by a sharp increase of the number of Si atoms released at the beginning of the dissolution. Figures 3a and 5b show this increase as a function of the advancement of the dissolution reaction. Depending on the volumes, the advancements corresponding to this stage are different. However, a clear pattern is highlighted when this evolution is considered as a function of the number of iteration steps (i.e., time) (Figure 7a). The dissolution rate is always at maximum around the same iteration (≈8000th) for the different volumes.

https://doi.org/10.1021/acs.jpcc.0c11416
J. Phys. Chem. C XXXX, XXX, XXX−XXX

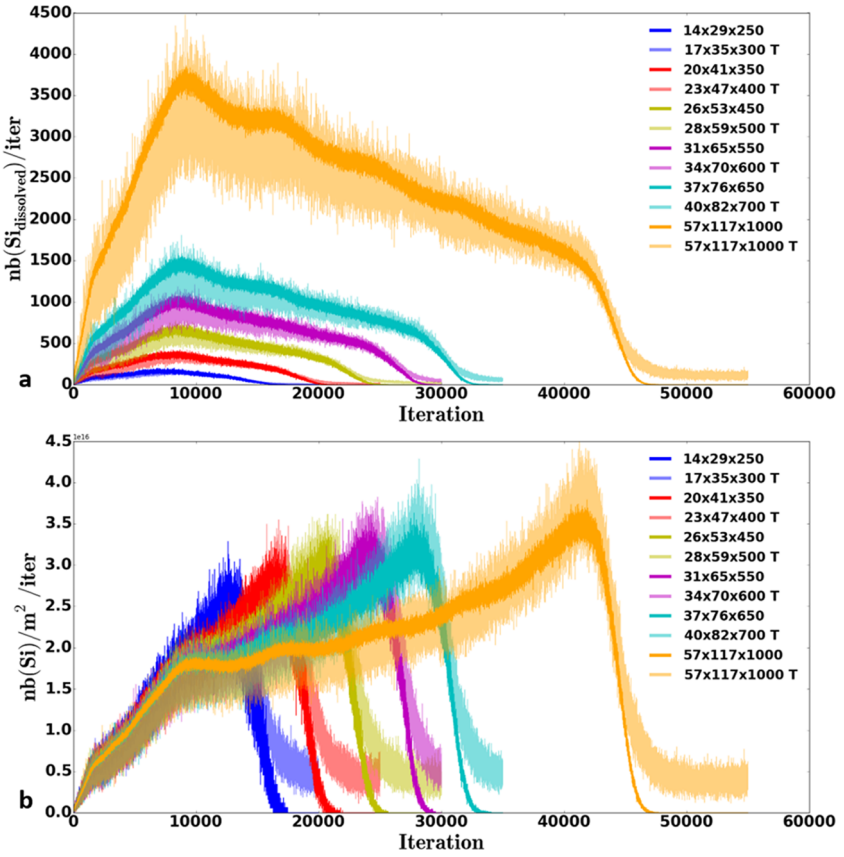

Figure 7. (a) Dissolution rate as a function of the total number of iteration steps (equivalent to time). Legends indicate how many times the crystal cell is multiplied in the *x*, *y*, and *z* directions. Light-colored curves represent the evolution of the number of Si atoms released per iteration based on theoretical considerations developed in Section 4.2. Dark-colored curves represent the simulation results of the stochastic dissolution of rectangular parallelepipeds. (b) Dissolution flux as a function of the total number of iteration steps. Light-colored curves represent the evolution of the number of Si released per iteration and per surface unit based on theoretical considerations developed in Section 4.2. Dark-colored curves represent the simulation results of the stochastic dissolution of rectangular parallelepipeds. In each panel, the agreement between theory and simulation outputs highlights the slight effects of edges and corners on the global rate/flux. The difference between theory and simulation outputs at the end of the simulations is due to the assumptions underpinning the theoretical model (see text for details).

Interestingly, this value corresponds to the one where the surface retreat of the (001) face reaches the steady state when the set of probabilities used is [0.99, 0.4, 0.0146] for [Mg−O−Mg, Si−O−Mg, Si−O−Si] bonds respectively.[16] It was interpreted as the moment when the dissolution becomes congruent. Considering that the other faces reach their steady-state dissolution regime before the (001) face,[16] the fact that the dissolution rate of the simulated rectangular parallelepipeds is at maximum at the iteration corresponding to the attainment of a steady state for face (001) may mean that the evolution of the dissolution regime of a simulated rectangular parallelepiped enstatite is controlled by the face for which this steady state is reached the latest (after the largest number of iterations). Alternatively, another explanation could be that the face (001) being the fastest to dissolve, the amount of Si released from this face is greater than those of the other faces. Hence, this relation between a simulated rectangular parallelepiped enstatite and the (001) face reaching their steady state at the same iteration may come from the fact that a significant proportion of their dissolution is supported by the (001) face.

Regarding the dissolution rate of Mg atoms, Figure 4 shows that it decreases dramatically during the first few hundred iterations (325 for the volume 40 × 82 × 700). This can be explained by the fast departure of Mg atoms from the reactive surface at the beginning of the simulations because of their greater probability to be dissolved. This results in a fast leaching step at the beginning of the reaction, when these atoms are numerous. After a few iterations, the main coordination of Mg at the surface increases prior reaching a constant value,[41] making them more difficult to dissolve.

The fast decrease of Mg dissolution rate can also be linked to the increase of Si dissolution rate. Indeed, the fewer the Mg−O−Si bonds, the higher the Si departure probability. In other words, when numerous Mg atoms are released into solution, the dissolution of Si atoms is enhanced. This departure of Si atoms resulting from the fast leaching of Mg atoms at the surface also makes it easier for the "solution" to reach the Mg atoms located deeper in the simulated crystals. These combined effects possibly explain why, after a dramatic decrease, the Mg dissolution rate increases with Si dissolution, until the maximum is reached. After the maximum is reached, both Si and Mg dissolution rates decrease. More importantly, these decreases are almost identical (same slope), indicating that the dissolution is stoichiometric.

4.1.2. Parameters Controlling the Dissolution. Although the first set of simulated rectangular parallelepipeds was not representative of the aspect ratio of natural enstatite grains,[50] it allows highlighting some behaviors and parameters that may control the dissolution. Indeed, the two subgroups presented in Figure 3 have their own patterns that can help understand the

https://doi.org/10.1021/acs.jpcc.0c11416
J. Phys. Chem. C XXXX, XXX, XXX−XXX

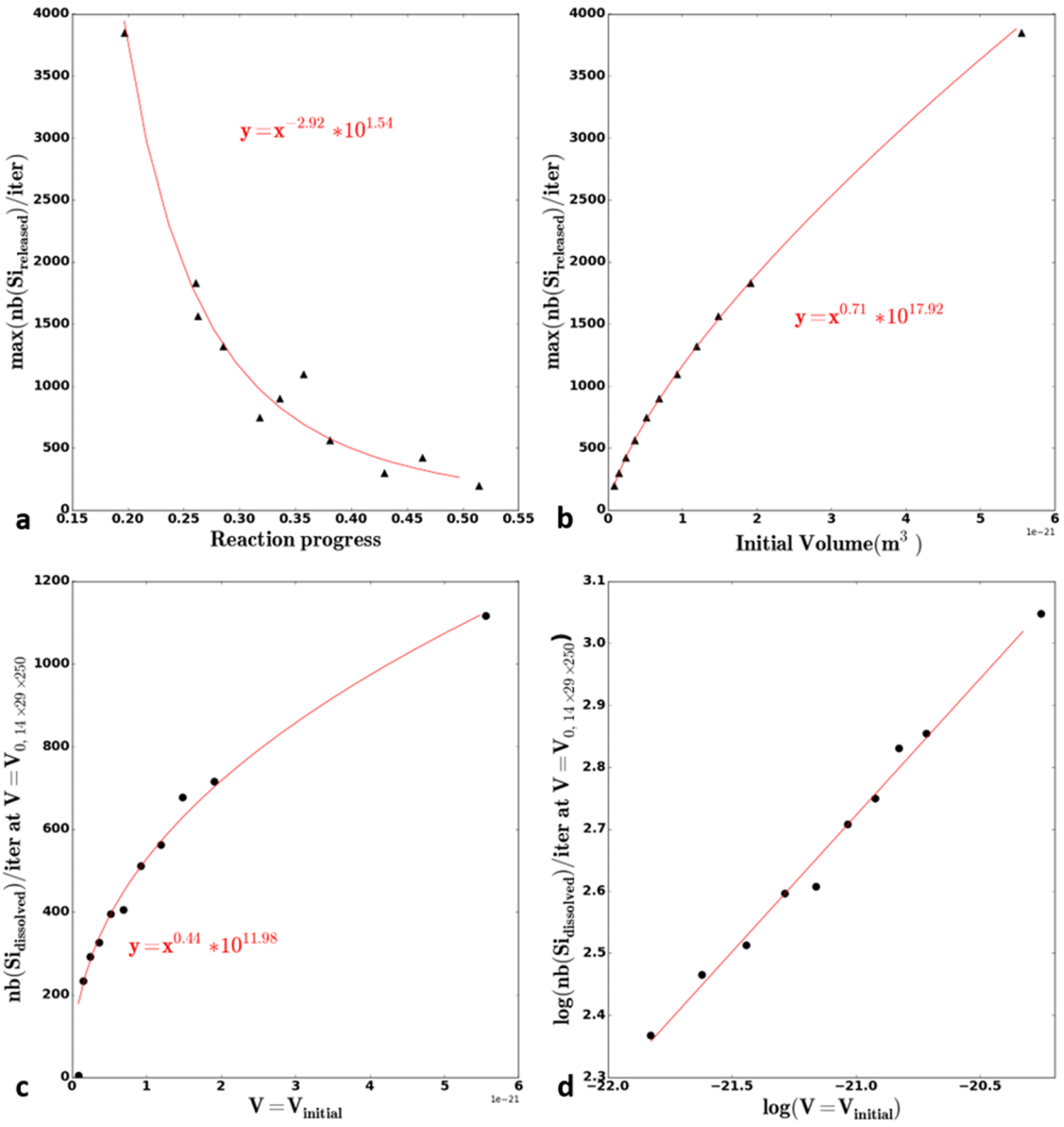

Figure 8. (a) Maximum dissolution rate as a function of the progress of the dissolution process for various initial volumes. Each triangle represents a different initial volume. The maximal value corresponds to the largest volume and the minimal to the smallest. (b) Maximum dissolution rate as a function of the initial volume. (c, d) Dissolution rate when the volume of the enstatite grain reaches the initial volume of the smallest simulated rectangular parallelepiped ($14 \times 29 \times 250$) as a function of the initial simulated enstatite rectangular parallelepiped volume represented in standard and logarithmic scales, respectively.

two principal factors impacting the dissolution, namely, the length of the rectangular parallelepiped in the *z*-direction and the surface area of the (001) face. The most striking feature is the one of the subgroup composed of rectangular parallelepipeds varying only by their heights ($40 \times 75 \times 250$, $40 \times 75 \times 300$, $40 \times 75 \times 350$, $40 \times 75 \times 400$, $40 \times 75 \times 450$, and $40 \times 75 \times 500$). While the beginning of the dissolution differs depending on the volume, the stage depicting a decreasing reactivity is characterized by a similar trend and value of Si dissolution rates for all simulations (Figure 3b). Therefore, it can be assumed that this stage is controlled mostly by the surface area of the (001) faces. Then, the surface area of the (100) and (010) faces would only affect the reaction progress required to reach this stage (the greater these surfaces, the longer the preliminary stage).

This assumption can be verified with the second subgroup of simulated rectangular parallelepipeds ($50 \times 103 \times 176$, $75 \times 150 \times 75$, $150 \times 75 \times 75$, $90 \times 90 \times 180$, and $120 \times 120 \times 120$). Indeed, the only simulations presenting the same (001) surface area are those conducted with the $75 \times 150 \times 75$ and $150 \times 75 \times 75$ volumes. These two rectangular parallelepipeds have the same dissolution behavior throughout the entire reaction (Figure 3a). While this similarity supports that the dissolution is primarily controlled by the face (001), it also suggests that the other two faces have only a minor contribution to the overall dissolution rate of enstatite grains. This is further supported by the differences in reaction rates between the three faces ((100), (010), and (001)). The dissolution rate of the (001) face is more than 1 order of magnitude higher than those of faces (100) and (010). To have a significant impact on the total dissolution rates, the surface area of the (100) and (010) faces should be at least

https://doi.org/10.1021/acs.jpcc.0c11416
J. Phys. Chem. C XXXX, XXX, XXX−XXX

10 times greater than that of the (001) face, which was never investigated in this study due to computational capacities and our commitment to perform simulations that observe as much as possible the aspect ratios of enstatite grains encountered in natural environments.

The difference in shape between the released Si curves of the two subgroups (Figure 3a vs Figure 3b) is more difficult to explain. The main difference in the simulation parameters resides in the dimensions of the simulated volumes and mainly, their heights. Indeed, the heights (length in the z direction) of the subgroup composed of the $50 \times 103 \times 176$, $75 \times 150 \times 75$, $150 \times 75 \times 75$, $90 \times 90 \times 180$, and $120 \times 120 \times 120$ rectangular parallelepipeds are smaller than those of the volumes of the second subgroup. It is therefore possible that the former volumes are consumed before reaching a stage where the Si dissolution rate decreases linearly, which would explain this difference in behavior. If the overall dissolution is mainly controlled by the dissolution of the (001) faces, it is indeed possible that these volumes cannot reach this dissolution stage because their height is too short. This is consistent with the evolution of the dissolution rate of the other subgroup for which the smaller the volume, the shorter the linear stage. It can be reasonably assumed that rectangular parallelepipeds with a very short height never reach a stage where the dissolution rate decreases linearly.

To conclude, the simulations shown in Figure 3 provide important information regarding the global dissolution of a rectangular parallelepiped enstatite: the dissolution rate seems mainly controlled by that of the (001) faces.

The simulations conducted with the second set of rectangular parallelepipeds, more representative of the natural crystal habit of pyroxenes, also exhibit specific patterns. Indeed, while the amount of Si atoms released at each iteration varies from one volume to another, trends and shapes are identical (Figure 5). This could indicate that the overall evolution of the dissolution is directly controlled by the shape of an enstatite grain. For the same aspect ratio, the initial volume only influences the absolute amount of released atoms.

This simulation set allows focusing on a quantity that delineates a transition in the evolution of the dissolution rate of a rectangular parallelepiped enstatite, namely, the maximum value this latter can reach (black triangles in Figure 5a). While it is obvious that the bigger the volume of a rectangular parallelepiped, the greater the instantaneous Si dissolution rate, interestingly, it is possible to link these two quantities mathematically (Figure 8b). In the same way, it is possible to link this maximum rate to the reaction progress (Figure 8a). The corresponding relations are given by

$$\max(\mathrm{Si}_{\mathrm{released}}) = 10^{17.9} \times V_0^{0.71}$$

$$\max(\mathrm{Si}_{\mathrm{released}}) = 10^{1.54} \times \xi^{-2.92} \quad (6)$$

where V_0 is the initial volume (m^3) and ξ is the reaction progress.

Combining these two relations allows predicting the reaction progress corresponding to the maximal dissolution rate as a function of the initial volume.

$$\xi_{\max(\mathrm{Si})} = 10^{-5.61} \times V_0^{-0.24} \quad (7)$$

Based on this equation, it is theoretically possible to estimate the time at which the release of Si is maximal when knowing the initial volume of an enstatite grain. Such empirical relations are very relevant for experimental works and practical applications because it corresponds to the attainment of the steady-state regime of the dissolution (see Section 4.5).

4.1.3. Variability of Dissolution Rates for a Given Grain Size. A long-standing concern in mineral/water interaction deals with the uniqueness of the dissolution rate.[18,51] While the variability of the dissolution rate is known to be significant when the geochemical conditions are changed, it is often assumed, particularly in reactive-transport studies, that the intrinsic dissolution rate constant remains unchanged when the fluid chemistry and the temperature are constant. However, several studies tend to show that this assumption may be too simplistic, as the dissolution rate may vary with time. While some studies highlight a monotonic decrease of the dissolution rate with time which can be associated with several factors such as the development of amorphous silica-rich layers,[52] others emphasize a complex evolution of the dissolution rate resulting from the gradual modification of the crystal habit,[15,23,53] the inherited history of the crystal reactivity[54,55] or the microstructural differences (e.g., defect density) between two individual crystals of a same mineral.[3,5,18,23,56−58] Therefore, it is central to understand if two minerals placed under the same biogeochemical conditions but differing in their history (one being fresh and the other one being aged for example) will have the same dissolution rate; hence, if two minerals of the same volume have the same unique dissolution rate.

To investigate this question using the dissolution model, it has been decided to focus on the dissolution rate of the rectangular parallelepipeds when their volume reaches a volume equivalent to that of the smallest simulated crystal ($14 \times 29 \times 250$). The remaining volume is calculated with the number of atoms that are still in the rectangular parallelepiped at each iteration following

$$V_i = \frac{a^*b^*c}{16}\left(N_0 - \sum_i^{n=0} N_n\right) \quad (8)$$

with V_i the volume at the ith iteration; a, b, and c the cell parameters (m); N_0 the number of Si atoms in the enstatite parallelepiped at the beginning of the simulation; and N_n, the total number of Si released until the ith iteration. This mass balance is divided by 16 since the enstatite cell is formed by 16 atoms of Si. The attainment of the volume corresponding to the smallest crystal is indicated by the black circles in Figure 5, and the dissolution rates at $V = V_{14\times29\times250}$ (named $\mathrm{Si}_{\mathrm{released},\ V=V_{14\times29\times250}}$) as a function of the initial volume are shown in Figure 8c,d. Interestingly, a relation between the initial volume and the dissolution rates for $V = V_{14\times29\times250}$ exists

$$\mathrm{Si}_{\mathrm{released},\ V=V_{14\times29\times250}} = 10^{12.0} \times V_0^{0.44} \quad (9)$$

This kind of relationships means that for a given volume, different values of dissolution rates exist depending on the initial size of the minerals.

4.2. Simple Mathematical Model of Si Dissolution Rate. The evolution of Si dissolution rates and fluxes has a specific behavior as described above. If this behavior seems difficult to reproduce with a theoretical model, it is possible to test hypotheses on how the dissolution evolves: here, we suggest testing the assumption that the overall enstatite grain dissolution simply corresponds to the sum of the contribution of the various single faces delineating the enstatite volume. This assumption may be true if, contrary to what is often proposed in the literature, the edges and corners do not have a strong impact on

https://doi.org/10.1021/acs.jpcc.0c11416
J. Phys. Chem. C XXXX, XXX, XXX−XXX

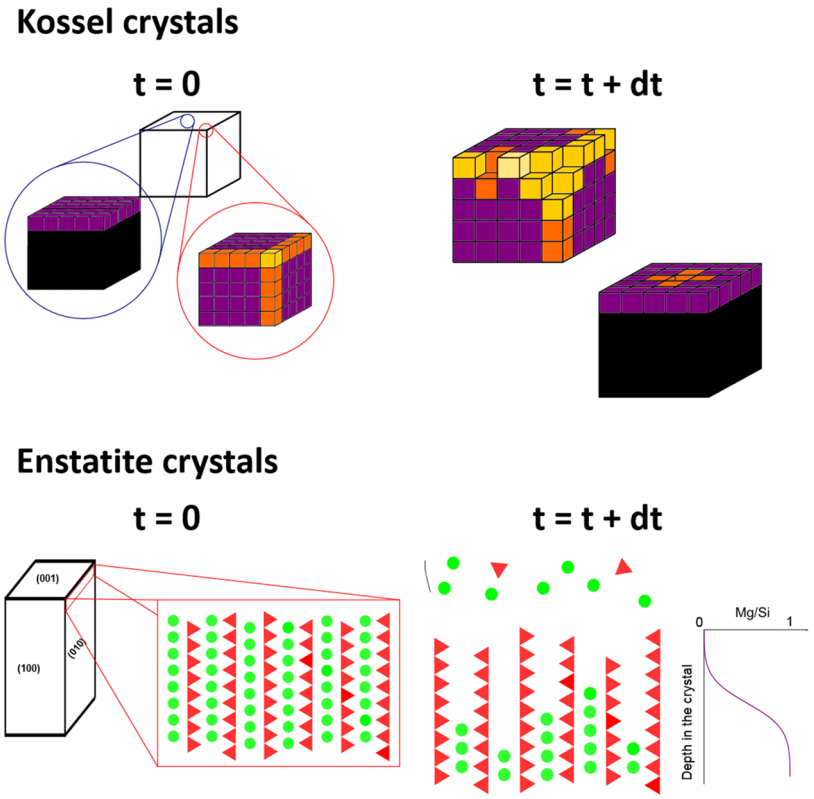

Figure 9. Scheme of the mechanism driving the dissolution of Kossel and enstatite crystals. Kossel: Black cubes represent atoms that are not at the mineral reactive surface. Purple, orange, and yellow cubes represent surface-, edge-, and corner-site atoms, respectively. During the dissolution, the atoms with fewer neighbors have a higher probability to be dissolved. This leads to the formation of rounded corners and edges. The atoms at the surface with only one neighbor missing (purple) are particularly difficult to dissolve compared to the others. Enstatite: at the beginning of the dissolution, Mg atoms are dissolved first. This is particularly visible on the (001) face where they exhibit a less populated first coordination sphere, leading to Mg depletion of the surface and the formation of a Si-enriched layer with a thickness not exceeding a few atomic layers. Because silica chains are not connected to each other, the probability of departure of Si atoms is the same on the entire (001) face, making it unlikely to exhibit rounded edges and corners.

the dissolution rate/flux and thus, if these sites do not lead to an excessive rounding of the crystal. In this case, a simple cross-multiplication would be able to reproduce the evolution of the dissolution rate/flux.

To model the dissolution of Si atoms, the first step is to consider the volume (ΔV_i) that is dissolved during an iteration

$$\Delta V_i = V_{i-1} - V_i \tag{10a}$$

$$V_i = (x_0 - 2\Delta h_i^{(100)})(y_0 - 2\Delta h_i^{(010)})(z_0 - 2\Delta h_i^{(001)}) \tag{10b}$$

If the dissolved volume is known, the number of Si atoms released per iteration can easily be calculated knowing the volume of the enstatite cell and the number of Si atoms it contains (16)

$$\mathrm{Si}_{\mathrm{released},i} = \frac{16\Delta V_i}{abc} \tag{11}$$

Modeling the release rate of Si requires to know the values of $\Delta h_i^{(hkl)}$ at each iteration step i, which requires to know the face-specific dissolution rate of enstatite both at steady state and during the transient states, i.e., at the beginning and at the end of the simulations. To the best of our knowledge, while an analytical expression has been developed in Bouissonnié et al.[41] for the steady state, a similar expression does not exist for transient phases. To model the dissolution of the rectangular parallelepipeds used in the different simulations, we first performed three additional face-specific simulations (i.e., simulations where only the atoms belonging to the face (hkl) are allowed to react, thus excluding atoms belonging to edges, corners, and all other ($h'k'l'$) faces), with a depth equivalent to half the depth of the volume in a given direction. The evolution of the surface retreats as a function of time for the (100), (010), and (001) faces were then retrieved and implemented in eq 10b to model the dissolution of a rectangular parallelepiped and determine the evolution of the release rate of Si atoms as a function of time. The results of this dissolution model are presented in Figure 7 (light-colored curves) and compared to the outputs of the simulations conducted with rectangular parallelepipeds (dark-colored curves). The agreement between both models is striking, with a sharp increase of the dissolution rate observed during the first 8000 iterations, followed by a slow decrease of the dissolution rate and a sharper decrease at the end of simulations.

4.3. Comparison between Results of the Simulation and Modeled Dissolution. Figure 7 shows that the results derived from theoretical dissolution and modeled dissolution are almost identical. With the exception of the very end of the dissolution, the results of the simulations performed with rectangular parallelepipeds and those derived from face-specific dissolution are superimposed. However, contrary to the results of the simulations performed with rectangular parallelepipeds, those derived from face-specific dissolution exhibit a greater standard variation around the mean value of the curves. This

https://doi.org/10.1021/acs.jpcc.0c11416
J. Phys. Chem. C XXXX, XXX, XXX−XXX

observation stems from the fact that stochastic variations in the instantaneous dissolution rate of each single face are cumulated, increasing the overall standard variation artificially. Interestingly, when one looks at the variation of the dissolution rate as a function of the number of elapsed iterations (Figure 7a), the mean value of the results derived from the face-specific approach is slightly lower than the one derived from the simulations performed with rectangular parallelepipeds. This slight difference may be explained by the contribution of corners and edges to the dissolution rate/flux. However, contrary to other minerals, the dissolution of these surface sites seems to have a negligible impact. A scheme exhibiting the difference between enstatite and a Kossel crystal[9,19,36,37,59−61] dissolution, for which the contribution of edges and corners was shown in previous studies to be significant, is depicted in Figures 9 and 10 to explain this counterintuitive result. These schemes are based on the periodic bond chain theory,[17] which governs silicate dissolution. In a Kossel crystal, the volume is composed of a unique component ("atom"), leading to the existence of a single type of bond. By nature, a Kossel crystal will have specific surface sites (adatoms, steps, and kinks) with a high probability of departure, leading to the rounding of the simulated crystals over time. In the case of enstatite, the anisotropic nature of pyroxenes makes this morphological evolution simpler. As opposed to, e.g., tectosilicates, which have a three-dimensional framework of silica tetrahedrons, inosilicates are composed of silica chains oriented following a specific direction (parallel to the *c*-axis in enstatite). In enstatite, Mg and Si atoms are also organized in planes parallel to the (100) face. This particular organization explains the anisotropy of dissolution of enstatite, as discussed in Bouissonnié et al.,[16] and likely explains why macro steps and corners do not play an essential role in the evolution of the dissolution rate with time. Indeed, as shown in Figure 9, most of enstatite dissolution flux is supported by (001) faces. This is due to the fact that the release of Si from (*hk*0) faces requires the simultaneous cleavage of two Si−O−Si bonds, while the release of Si from (001) faces requires the cleavage of one Si−O−Si bond only.

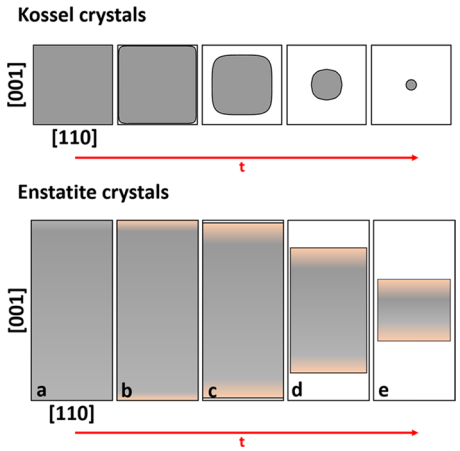

Figure 10. Scheme of the effect of dissolution through time on Kossel and enstatite crystals. Kossel: the high probability of departure of edge and corner sites leads to a rounding of the corresponding locations. This modifies significantly the crystal shape during the dissolution, which evolves from a cubic to a spherical shape. Black squares represent the crystal shape at $t = 0$. The gray area represents a section of the crystal. Enstatite: At the beginning of the dissolution, Mg atoms are preferentially dissolved due to their particularly incomplete first coordination sphere, leading to the formation of a Si-enriched layer (orange area) on the (001) face (a−c). The Si-enriched layer reaches its constant depth (b, c) and the dissolution becomes stoichiometric. Both Si and Mg atoms are dissolved preferentially on the (001) face, but a few are dissolved on the (100) and (010) faces (c−e). This dissolution behavior makes the rounding of the crystals unlikely.

This specific anisotropic structure also explains why the model depicted in Section 4.2 successfully matches the outputs of the simulations run with enstatite parallelepipeds, indirectly suggesting that no rounding of the crystals occurs with time. The greater probability to release Mg atoms to the solution results in the formation of a Mg-depleted zone at the mineral surfaces during the first iterations (Figure 4), where the mineral−solution interface is only composed of chains of Si atoms (Figure 9). This process is more pronounced at the surface of the (001) faces, where Mg atoms have the greater departure probabilities. This is fully consistent with the experimentally observed thicker amorphous silica layers on (001) faces. If the (001) faces exhibit a Mg-depleted mineral−solution interface, then it means that it is composed essentially on silica chains, not connected between them (Figure 9). These silica chains will be present throughout the entire surface of the (001) face but, as their topmost Si atoms all exhibit the same departure probability, a rounding of the edges and kinks is unlikely to happen.

In summary, the dissolution of a Kossel crystal can be described as follows: (i) Initial fast release of atoms from the kinks and edges of the minerals; (ii) Through time, the Kossel crystal habit evolves from a cubic to an almost spheroidal shape. Conversely, the dissolution behavior of enstatite and more generally, of pyroxenes, can be summarized as follows: (i) Rapid depletion of the topmost Mg atoms from the (001) faces; (ii) stabilization of the thickness of the corresponding silica layer; and (iii) propagation of the dissolution front mainly from the (001) faces. These mechanistic explanations are summarized in Figures 9 and 10. Also, as mentioned in Section 2.4, the model is not able to reproduce the amorphous silica layer. Then, the interface mainly composed of Si atoms remains "crystalline" with only disconnected silica chains. This may present a limitation to the mechanisms developed above as, in natural environment, a thicker amorphous silica layer may impact the crystal shape evolution. Extending this discussion to other minerals requires a specific treatment of other classes of minerals, which is out of the scope of this study. However, it is likely that many minerals, which highlight an anisotropy similar to pyroxenes could observe a similar dissolution mechanism. One could argue that many minerals are more anisotropic than enstatite because of its orthorhombic Bravais lattice, which has a high symmetry level. However, the notion of anisotropy here refers to the organization of the Si tetrahedrons. In this regard, orthorhombic inosilicates are less isotropic than, e.g., triclinic tectosilicates, which have a three-dimensional framework of silica tetrahedrons, even though the symmetry level of the orthorhombic system is higher than that of the triclinic system.

Finally, the main discrepancy between model's outputs and theoretical results is observed at the end of the simulations. While the dissolution rates calculated using the simulations run with rectangular parallelepipeds reach 0 at the end of the reaction, indicating that all of the material is consumed, it is not the case for the rates calculated based on face-specific dissolution rates and using eqs 10a and 10b. This observation is an artifact resulting from the mathematical construction of the model. While faces (100), (010), and (001) are considered, the

https://doi.org/10.1021/acs.jpcc.0c11416
J. Phys. Chem. C XXXX, XXX, XXX−XXX

dissolution is mainly controlled by the sole (001) face. Equation 10b implies that all faces dissolve independently so that when the length of the parallelepiped following the z-axis reaches 0, it is not the case for the two other axes. Therefore, following eq 10b, a plan of enstatite contained in the two-dimensional (2D) (xOy) plan still exists and continues to fuel the dissolution. Conversely, in the real world (and in the simulations run with rectangular parallelepipeds), the dissolution stops when the crystal is completely dissolved.

4.4. Comparing Modeled Dissolution Fluxes and Experimental Results. *4.4.1. Comparison Based on Dissolution Experiments Conducted with Powdered vs Single-Face Enstatite.* In the previous section, it has been shown that it is possible to reproduce the grain dissolution behavior with a simple mathematical model considering the dissolution fluxes of the faces in contact with the fluid. However, this good agreement was obtained using simulation results only. While, theoretically, the model used in the present study is also able to reproduce experimental data,[16] the corresponding validation has been previously based on a comparison with measured face-specific dissolution fluxes only, and not with results from powder experiments. This missing comparison is therefore attempted hereafter. As a first step, we use below the additivity property of single-face dissolution fluxes illustrated in Section 4.3 to compare the results of dissolution experiments previously conducted with single faces with those conducted with powdered enstatite.

In their study, Oelkers and Schott[11] have determined the dissolution flux of enstatite powder over a wide range of pH and temperature. Using the reaction order with respect to $[H^+]$ and the activation energy derived from their study, the dissolution flux of enstatite powder at 90 °C and pH 0 (the chemical conditions simulated in this study) should be around 2.35×10^{-8} mol/(m^2 s). In our previous study, the different dissolution fluxes of the four main faces naturally exposed in enstatite have been determined to yield 5.22×10^{-9}, 5.92×10^{-9}, 1.7×10^{-8}, and 1.44×10^{-7} mol/(m^2 s) for the faces (100), (010), (210), and (001) respectively[16] (note that the results of Bouissonnié et al.[16] were corrected by a 2-fold factor, as they considered $Mg_2Si_2O_6$ as the chemical formula for enstatite, whereas Oelkers and Schott used $MgSiO_3$). The main cleavage plan of enstatite is {210}[62] and is likely to be the most abundant when enstatite is crushed prior to run powder dissolution experiments. If one assumes that, in enstatite powders, mostly (210) and (001) faces are present, then based on the results of the previous section, the dissolution flux of the powder can be calculated following:

$$r = \frac{4*S_{(210)}*r^{(210)} + 2*S_{(001)}*r^{(001)}}{S_0} \quad (12)$$

where $S_{(hkl)}$ is the surface area of the (hkl) face (m^2), $r^{(hkl)}$ is the dissolution flux (mol/(m^2 s)) of the (hkl) face, and S_0 is the initial surface area (m^2). Depending on the size of the grains used in this calculation ($10 \times 10 \times 100$ or $20 \times 20 \times 100$ μm^3, consistent with the grain size range reported in the Oelkers and Schott study), the dissolution flux is estimated to be 2.85×10^{-8} and 2.31×10^{-8} mol/(m^2 s) for $20 \times 20 \times 100$ and $10 \times 10 \times 100$ μm^3 crystals, respectively. These values are in excellent agreement with the dissolutions flux calculated based on the study of Oelkers and Schott (hereafter referred to as r_{OS}) (2.35×10^{-8} mol(m^2 s)). This agreement further supports that edges and corners must negligibly contribute to the dissolution flux of enstatite grains, consistent with the previous section.

4.4.2. Testing Different Methods to Upscale Dissolution Fluxes from Face-Specific Simulations to Powder Dissolution Experiments. The ability of the model to reproduce dissolution fluxes derived from powder experiments with dissolution fluxes derived from face-specific simulations and experiments has been shown in Sections 4.3 and 4.4.1, respectively. However, simulating directly the dissolution of entire crystals with dimensions of typical grains used in laboratory experiments remains out of reach with current numerical methods. Indeed, our computational capabilities allow us to simulate the dissolution of crystals up to $0.1 \times 0.1 \times 1$ μm^3, whereas the typical enstatite grain size for powder dissolution experiments[11,50] is on the order of $10 \times 10 \times 100$ μm^3.

To circumvent this problem, a solution is to consider the good agreement between the results of the simulations run with rectangular parallelepipeds and the results calculated using face-specific dissolution (eq 10a). As the surface retreat does not depend on the considered surface area, each of the three main phases of the dissolution of a given face (i.e., initial transient regime, steady-state regime, i.e., linear increase of the surface retreat with iterations, and terminal regime) extends over a similar number of iterations, whatever the surface area considered. We used this property to simulate the dissolution of crystals with dimensions approaching those of grains used in classical powder dissolution experiments (see Figure 11). This process is repeated for all faces to simulate the dissolution of an entire parallelepiped. The results of the simulations conducted with this large volume are shown in Figures 5b and 6b (black curves). This process allows studying the evolution of the dissolution behavior over a wide range of volumes and also to understand how such systems evolve. Ultimately, the simulation of such large volumes allows comparing modeled and experimental data.

The first important highlight is that no real steady state is reached for dissolution rate/flux (Figures 5b and 6b). Indeed, the dissolution rate and flux steadily increase over the course of the simulation. This may be due to the evolution of the surface area that is not correctly captured, as the calculation does not consider its intrinsic variability over the entire surface (intrinsic reactivity and etch pits formation for example). However, the increase is slow and not significant (below 14 nmol/s, which would remain out of reach of conventional techniques used to measure dissolution fluxes in the laboratory), and this regime can therefore be approximated to a steady state. This pseudo-steady state corresponds to a mean dissolution flux of approximately 1.8×10^{16} Si atoms/(m^2 iteration) which yields 2.62×10^{-8} mol/(m^2 s), if one applies the time/iteration relationship calculated by Bouissonnié et al.[16] (r(mol/(m^2 s)) = $0.876 \times r$(mol/(m^2 iteration))). This value is in very good agreement with that determined by Oelkers and Schott (~1.11 r_{OS}).

Three additional upscaling methods are tested and compared with r_{OS}.

The first method consists of considering the dissolution fluxes determined with single-face dissolution experiments:[16] (a) with faces (100), (010), and (001) and (b) with faces (210) and (001)

https://doi.org/10.1021/acs.jpcc.0c11416
J. Phys. Chem. C XXXX, XXX, XXX−XXX

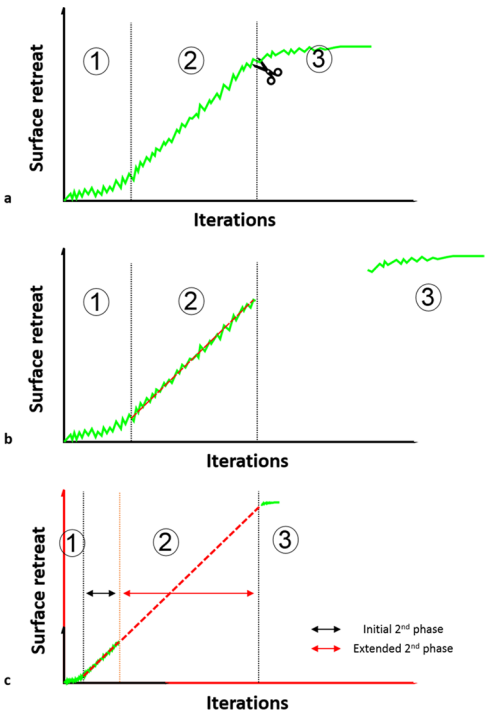

Figure 11. Scheme of the method followed to get the dissolution flux of enstatite rectangular parallelepipeds with a size comparable to those used in Oelkers and Schott.[11] (a) Surface retreat simulated as a function of the iterations is used for each considered face (e.g., (100), (010), and (001)). It is divided into three different phases: (1) the transient regime, (2) the steady-state regime, and (3) the terminal regime, corresponding to the consumption of the remaining atoms in the materials. A cut is operated between the second and third phases. (b) A linear regression (dashed red line) is applied, based on the results of the steady-state phase starting from the transition between the first and second phases and ended between the second and third phases. (c) Linear regression is used to increase the size of the parallelepiped to reach the size used by Oelkers and Schott. The third phase is then added at the end of the extended second phase.

$$r = \frac{16^*\Delta V(\Delta t)}{a^*b^*c^*\Delta t^*S_0^*N_A}$$

$$\Delta V(\Delta t) = V_t - (x_t - 2\Delta h_{\Delta t}^{(100)|(210)})(y_t - 2\Delta h_{\Delta t}^{(010)|(210)})(z_t - 2\Delta h_{\Delta t}^{(001)}) \quad (13)$$

where r is the dissolution flux (mol/(m^2 s)), Δt is the time interval considered for the calculation (s), S_0 is the initial surface (m^2), N_A is the Avogadro number (mol^{-1}), $\Delta V(\Delta t)$ is the difference of volumes over the time interval Δt (m^3), and $\Delta h_{\Delta t}^{(hkl)}$ is the surface retreat of the (hkl) face over the time interval Δt.

The second method uses the surrogate relation between the dissolution flux and the probabilities (i.e., activation energies) determined in Bouissonnié et al.[41]

$$\frac{\Delta h_{(hkl)}}{\Delta t} 0.876 \begin{bmatrix} kP_{Mg-O-Mg}^{\alpha} P_{Mg-O-Si}^{\beta} P_{Si-O-Si}^{\gamma} + \\ k_{dis} P_{Mg-O-Mg}^{\alpha_{dis}} P_{Mg-O-Si}^{\beta_{dis}} P_{Si-O-Si}^{\gamma_{dis}} (1 - e^{-\rho_d/\omega}) \end{bmatrix} \quad (14)$$

with k, k_{dis}, α, β, γ, α_{dis}, β_{dis}, γ_{dis}, and ω being empirical parameters and ρ_d the dislocation density. The left-hand side of the sum referred to the "bulk" dissolution flux, while the right-hand side referred to the contribution etch pits at dislocation outcrops. The values of these parameters were determined in Bouissonnié et al.[41] and are listed in Table 1.

Table 1. Numerical Values of the Parameters in Equation 12 and Taken from Bouissonnié et al.[41] [a]

face	(100)	(010)	(001)
k (Å/it)	8.87	7.8	4.72
α	2.46	2.22	6.36
β	4.62	4.65	4.19
γ	0.94	0.75	0.14
k_{dis} (Å/it)	44.7	44.7*	
α_{dis}	2.09	2.09*	
β_{dis}	4.09	4.09*	
γ_{dis}	0.67	0.67*	
ω	5.51×10^{10}	5.51×10^{10}*	
ρ_d (/cm^2)	4.9×10^8	9.8×10^6	0

[a] α, β, and γ represent fitting parameters for bulk dissolution rate (without the presence of dislocation). α_{dis}, β_{dis}, and γ_{dis} represent fitting parameters for dissolution rate impacted by the presence of dislocations. The parameters k and k_{dis} represent the dissolution constant for bulk dissolution rate and dissolution rate impacted by the dislocation, respectively. ω is a fitting parameter, and ρ_d is the dislocation density measured in Bouissonnié et al.[16] (*) Parameters corresponding to the presence of dislocation on the (010) face were not studied. For this study, it has been assumed that they were equal to those of the (100) face.

The last method considers the modeled face-specific dissolution fluxes given in Bouissonnié et al.[16]

The three methods were applied on $20 \times 20 \times 100$ and $10 \times 10 \times 100$ μm^3 rectangular parallelepipeds (considered as a model shape and size for the grains used in Oelkers and Schott[11,50]), and the results are summarized in Table 2. Overall, all methods exhibit a satisfactory agreement with the results obtained experimentally, with discrepancies never exceeding 50%. Of note, a better agreement is obtained when the {210} face is considered. This observation may confirm that enstatite grains were mainly shaped with {210} face in the powder used

Table 2. Numerical Values of the Steady-State Dissolution Flux of an Enstatite Grain Considering the Simple Relation between Face-Specific Dissolution Flux and Powder Dissolution Flux Following Several Methods[a]

method	crystal size (m^3)	dissolution flux (r = mol/(m^2 s)) ($\times 10^{-8}$)	r/r_{OS}
surface retreat of (100), (010), and (001)[16]	$20 \times 20 \times 100$ μm^3	1.78	0.76
	$10 \times 10 \times 100$ μm^3	1.18	0.50
surface retreat of (210) and (001)[16]	$20 \times 20 \times 100$ μm^3	2.75	1.17
	$10 \times 10 \times 100$ μm^3	2.17	0.92
surrogate model[41]	$20 \times 20 \times 100$ μm^3	2.22	0.94
	$10 \times 10 \times 100$ μm^3	1.62	0.69
this study	$20 \times 20 \times 100$ μm^3	2.62	1.11
single-face-modeled results[16]	$20 \times 20 \times 100$ μm^3	1.88	0.8
	$10 \times 10 \times 100$ μm^3	1.35	0.57

[a] The agreement (evaluated by the r/r_{OS} ratio) between powder dissolution experiments of Oelkers and Schott[11] and results obtained from face-specific dissolution experiments and modeling taken from Bouissonnié et al.[16,41] are reported in the last column. Crystal size has been chosen according to that reported in Oelkers and Schott, and an aspect ratio consistent with Dana.[50]

https://doi.org/10.1021/acs.jpcc.0c11416
J. Phys. Chem. C XXXX, XXX, XXX−XXX

by Oelkers and Schott, which is consistent with the fact that {210} represents the main cleavage plan of enstatite.

4.5. Relevance for Mineral Dissolution Studies and Limitations. Both experimental results obtained with face-specific dissolution measurements and those obtained with the stochastic dissolution model run with rectangular parallelepipeds succeed to reproduce the dissolution rates/fluxes measured during powder dissolution experiment. Here, we showed that face-specific and powder dissolution rates can be linked using a simple relation. However, this may be only true in the case of very anisotropic minerals such as enstatite (and pyroxenes) because edges and corners contribute negligibly to the dissolution flux. This conclusion does not hold for calcite, for example, as Noiriel et al.[25] showed that corners dissolve faster than (104) cleavage plans. In our opinion, our results would justify investigating the dissolution of other minerals according to the methods reported here to determine the crystallographic structures for which dissolution obeys relations similar to those evidenced for enstatite.

The results presented here may also be useful to model silicate weathering in natural environments. Subsurface environments present a wide diversity of textures, from porous to fractured media. Although fractured media should involve a preferential water/solid interaction of a limited number of mineral cleavage planes, porous media can exhibit a greater variety of mineral faces in contact with water. Actually, as a first approximation, micrometer-wide enstatite grains may be simplified as rectangular parallelepipeds made of (210) and (001) faces only, for which the length of the crystal in the z-direction is 5−10 times greater than in the other directions leading to consider the dissolution rate given by eq 12. This result may still hold true in less acidic environment as long as the fluid is far from equilibrium with respect to $SiO_{2(am)}$.[48] The fact that face-specific and powder dissolution studies can be linked through a simple relation for anisotropic minerals may imply that face-specific dissolution studies offer a greater interest than those conducted with powders for minerals presenting an anisotropy similar to the one of enstatite. In addition, our study shows the prevalence of fast dissolving faces over the others, suggesting that face-specific dissolution studies should target in priority such faces. Overall, the agreement between the outputs of the model and the theoretical results detailed in Section 4.2 shows how important it is to consider the evolution of the reactive surface area in geochemical/reactive-transport studies/models. The evolution of the aspect ratio was shown to be important in both cases when the reaction progress reaches approximately 80%. Indeed, at this step, the aspect ratio has evolved enough so that the reaction flux is characterized by a sharp increase. This may be of great interest to model chemical weathering in the regolith, where primary materials are altered into secondary minerals and may be the main contributors of dissolved elements in springs and rivers.

Interestingly, the simulated instantaneous release rates of Mg and Si atoms as a function of time (Figure 4) exhibit a specific shape that corresponds in every way to the calorimetry curves depicting the progress of cement hydration (cf. Figures 2−4 in Luc et al.[63]), for which the rate-limiting step is supposed to be the dissolution of silicate minerals such as alite. It is noteworthy that such a shape has puzzled the materials sciences community for a couple of decades, since it reveals a strong nonlinearity of the dissolution rate with time, which is at odds with existing models of mineral reactivity.[64] While previous attempts did not succeed to fully account for such observations,[65,66] the present study suggests that the anisotropic dissolution of silicates may indeed result in a general dissolution pattern consistent with previous measurements of cement hydration, representing relevant new avenues to be investigated in greater details.

Finally, among the main limitations of our study, the development of amorphous silica-rich surface layers through silica redeposition or surface network reorganization was not considered, as the impact of such layers is suspected to be nonsignificant in the experimental conditions investigated[3,47,67,68] by Bouissonnié et al.[16] (i.e., very acidic pH and low concentrations of aqueous silica). The implementation in the stochastic dissolution code of backward reactions of Si attachment, as described in, e.g., Zhang and Lüttge[69] or the consideration of M−O hydrolysis instead of M−O−M hydrolysis would be required to ultimately get closer to conditions operating in natural settings.

5. CONCLUSIONS

In this work, we simulated the dissolution of enstatite grains with a stochastic dissolution model developed at the atomic scale. By varying the size of the simulated grains, we showed that the main factor impacting the temporal evolution of the dissolution rate is the aspect ratio. A similar evolution of the dissolution rate through time is observed for grains with the same aspect ratio. Furthermore, different parameters such as the maximum dissolution rate, initial volume, dissolution at a given volume, and reaction progress were linked together through empirical functions.

One of the main outcomes of this study was provided by comparing the outputs of the stochastic grain dissolution with a theoretical dissolution model based on the sole contribution of face-specific dissolution, neglecting the contribution of edges and corners. The very good agreement between the two methods highlights the modest effects of edges and corners during enstatite dissolution, and probably, during the dissolution of other very anisotropic minerals as well (i.e., minerals where the stronger atomic bonds are aligned in a specific direction).

The comparison between modeled and experimental results obtained by Oelkers and Schott[11] on powder dissolution also revealed an excellent agreement. This led to the conclusion that powder dissolution results from the specific contribution of each face in a very simple way, making it possible to link the different experimental works performed in a laboratory.

Finally, this study shows the importance of fast dissolving faces. Indeed, almost the entire dissolution rate relies on the dissolution of the face (001). However, if the dissolution rates of the fastest dissolving faces are prominent, the overall dissolution rate is strongly correlated to the surface area of the other slower faces. This result supports the idea that reactive surface is one of the most important parameters in water/mineral interactions studies and that one must be aware, particularly in reactive-transport studies, of what is the reactive surface and how it should be taken into account.

AUTHOR INFORMATION

Corresponding Author

Arnaud Bouissonnié − *Laboratoire d'Hydrologie et de Géochimie de Strasbourg, Université de Strasbourg—CNRS/ENGEES—EOST, 67084 Strasbourg, France;* orcid.org/0000-0003-4590-5631; Phone: +33 (0)3 68 85 05 47; Email: arnaud.bouissonnie@etu.unistra.fr; Fax: +33(0)3 68 85 04 02

https://doi.org/10.1021/acs.jpcc.0c11416
J. Phys. Chem. C XXXX, XXX, XXX−XXX

Authors

Damien Daval − *Laboratoire d'Hydrologie et de Géochimie de Strasbourg, Université de Strasbourg—CNRS/ENGEES—EOST, 67084 Strasbourg, France;* orcid.org/0000-0002-4395-6681

Philippe Ackerer − *Laboratoire d'Hydrologie et de Géochimie de Strasbourg, Université de Strasbourg—CNRS/ENGEES—EOST, 67084 Strasbourg, France*

Complete contact information is available at: https://pubs.acs.org/10.1021/acs.jpcc.0c11416

Notes

The authors declare no competing financial interest.

■ ACKNOWLEDGMENTS

A.B. thanks the University of Strasbourg and CNRS for having funded his Ph.D. grant. The authors thank two anonymous reviewers for their helpful comments.

■ REFERENCES

(1) White, A. F.; Brantley, S. L. The Effect of Time on the Weathering of Silicate Minerals: Why Do Weathering Rates Differ in the Laboratory and Field? *Chem. Geol.* **2003**, *202*, 479−506.

(2) Daval, D.; Martinez, I.; Corvisier, J.; Findling, N.; Goffé, B.; Guyot, F. Carbonation of Ca-Bearing Silicates, the Case of Wollastonite: Experimental Investigations and Kinetic Modeling. *Chem. Geol.* **2009**, *265*, 63−78.

(3) Daval, D.; Hellmann, R.; Saldi, G. D.; Wirth, R.; Knauss, K. G. Linking Nm-Scale Measurements of the Anisotropy of Silicate Surface Reactivity to Macroscopic Dissolution Rate Laws: New Insights Based on Diopside. *Geochim. Cosmochim. Acta* **2013**, *107*, 121−134.

(4) Smith, M. E.; Knauss, K. G.; Higgins, S. R. Effects of Crystal Orientation on the Dissolution of Calcite by Chemical and Microscopic Analysis. *Chem. Geol.* **2013**, *360*−*361*, 10−21.

(5) Pollet-Villard, M.; Daval, D.; Fritz, B.; Knauss, K. G.; Schäfer, G.; Ackerer, P. Influence of Etch Pit Development on the Surface Area and Dissolution Kinetics of the Orthoclase (001) Surface. *Chem. Geol.* **2016**, *447*, 79−92.

(6) Saldi, G. D.; Voltolini, M.; Knauss, K. G. Effects of Surface Orientation, Fluid Chemistry and Mechanical Polishing on the Variability of Dolomite Dissolution Rates. *Geochim. Cosmochim. Acta* **2017**, *206*, 94−111.

(7) Godinho, J. R. A.; Piazolo, S.; Evins, L. Z. Effect of Surface Orientation on Dissolution Rates and Topography of CaF2. *Geochim. Cosmochim. Acta* **2012**, *86*, 392−403.

(8) Ruiz-Agudo, E.; King, H. E.; Patiño-López, L. D.; Putnis, C. V.; Geisler, T.; Rodriguez-Navarro, C.; Putnis, A. Control of Silicate Weathering by Interface-Coupled Dissolution-Precipitation Processes at the Mineral-Solution Interface. *Geology* **2016**, *44*, 567−570.

(9) Trindade Pedrosa, E.; Kurganskaya, I.; Fischer, C.; Luttge, A. A Statistical Approach for Analysis of Dissolution Rates Including Surface Morphology. *Minerals* **2019**, *9*, No. 458.

(10) Oelkers, E. H.; Schott, J.; Devidal, J.-L. The Effect of Aluminum, PH, and Chemical Affinity on the Rates of Aluminosilicate Dissolution Reactions. *Geochim. Cosmochim. Acta* **1994**, *58*, 2011−2024.

(11) Oelkers, E. H.; Schott, J. An Experimental Study of Enstatite Dissolution Rates as a Function of PH, Temperature, and Aqueous Mg and Si Concentration, and the Mechanism of Pyroxene/Pyroxenoid Dissolution. *Geochim. Cosmochim. Acta* **2001**, *65*, 1219−1231.

(12) Salehikhoo, F.; Li, L.; Brantley, S. L. Magnesite Dissolution Rates at Different Spatial Scales: The Role of Mineral Spatial Distribution and Flow Velocity. *Geochim. Cosmochim. Acta* **2013**, *108*, 91−106.

(13) Kurganskaya, I.; Luttge, A. A Comprehensive Stochastic Model of Phyllosilicate Dissolution: Structure and Kinematics of Etch Pits Formed on Muscovite Basal Face. *Geochim. Cosmochim. Acta* **2013**, *120*, 545−560.

(14) Perez, A.; Daval, D.; Fournier, M.; Vital, M.; Delaye, J.-M.; Gin, S. Comparing the Reactivity of Glasses with Their Crystalline Equivalents: The Case Study of Plagioclase Feldspar. *Geochim. Cosmochim. Acta* **2019**, *254*, 122−141.

(15) Pollet-Villard, M.; Daval, D.; Ackerer, P.; Saldi, G. D.; Wild, B.; Knauss, K. G.; Fritz, B. Does Crystallographic Anisotropy Prevent the Conventional Treatment of Aqueous Mineral Reactivity? A Case Study Based on K-Feldspar Dissolution Kinetics. *Geochim. Cosmochim. Acta* **2016**, *190*, 294−308.

(16) Bouissonnié, A.; Daval, D.; Guyot, F.; Ackerer, P. The Dissolution Anisotropy of Pyroxenes: Experimental Validation of a Stochastic Dissolution Model Based on Enstatite Dissolution. *J. Phys. Chem. C* **2020**, *124*, 3122−3140.

(17) Hartman, P. On the relations between structure and morphology of crystals. I. *Acta Cryst.* **1955**, *8*, 49−52.

(18) Arvidson, R. S.; Ertan, I. E.; Amonette, J. E.; Luttge, A. Variation in Calcite Dissolution Rates. *Geochim. Cosmochim. Acta* **2003**, *67*, 1623−1634.

(19) Briese, L.; Arvidson, R. S.; Luttge, A. The Effect of Crystal Size Variation on the Rate of Dissolution—A Kinetic Monte Carlo Study. *Geochim. Cosmochim. Acta* **2017**, *212*, 167−175.

(20) Kurganskaya, I.; Arvidson, R. S.; Fischer, C.; Luttge, A. Does the Stepwave Model Predict Mica Dissolution Kinetics? *Geochim. Cosmochim. Acta* **2012**, *97*, 120−130.

(21) Lasaga, A. C.; Luttge, A. Variation of Crystal Dissolution Rate Based on a Dissolution Stepwave Model. *Science* **2001**, *291*, 2400−2404.

(22) Fischer, C.; Luttge, A. Pulsating Dissolution of Crystalline Matter. *Proc. Natl. Acad. Sci. U.S.A.* **2018**, *115*, 897−902.

(23) Lüttge, A.; Arvidson, R. S.; Fischer, C. A Stochastic Treatment of Crystal Dissolution Kinetics. *Elements* **2013**, *9*, 183−188.

(24) Noiriel, C.; Oursin, M.; Saldi, G.; Haberthür, D. Direct Determination of Dissolution Rates at Crystal Surfaces Using 3D X-Ray Microtomography. *ACS Earth Space Chem.* **2019**, *3*, 100−108.

(25) Noiriel, C.; Oursin, M.; Daval, D. Examination of Crystal Dissolution in 3D: A Way to Reconcile Dissolution Rates in the Laboratory? *Geochim. Cosmochim. Acta* **2020**, *273*, 1−25.

(26) Kahl, W.-A.; Yuan, T.; Bollermann, T.; Bach, W.; Fischer, C. Crystal Surface Reactivity Analysis Using a Combined Approach of X-Ray Micro-Computed Tomography and Vertical Scanning Interferometry. *Am. J. Sci.* **2020**, *320*, 27−52.

(27) Luettge, A.; Bolton, E. W.; Lasaga, A. C. An Interferometric Study of the Dissolution Kinetics of Anorthite: The Role of Reactive Surface Area. *Am. J. Sci.* **1999**, *299*, No. 652.

(28) Bourg, I. C.; Steefel, C. I. Molecular Dynamics Simulations of Water Structure and Diffusion in Silica Nanopores. *J. Phys. Chem. C* **2012**, *116*, 11556−11564.

(29) Molins, S.; Trebotich, D.; Yang, L.; Ajo-Franklin, J. B.; Ligocki, T. J.; Shen, C.; Steefel, C. I. Pore-Scale Controls on Calcite Dissolution Rates from Flow-through Laboratory and Numerical Experiments. *Environ. Sci. Technol.* **2014**, *48*, 7453−7460.

(30) Steefel, C. I.; Appelo, C. A. J.; Arora, B.; Jacques, D.; Kalbacher, T.; Kolditz, O.; Lagneau, V.; Lichtner, P. C.; Mayer, K. U.; Meeussen, J. C. L.; et al. Reactive Transport Codes for Subsurface Environmental Simulation. *Comput. Geosci.* **2015**, *19*, 445−478.

(31) Kurganskaya, I.; Luttge, A. Kinetic Monte Carlo Simulations of Silicate Dissolution: Model Complexity and Parametrization. *J. Phys. Chem. C* **2013**, *117*, 24894−24906.

(32) Kurganskaya, I.; Luttge, A. Kinetic Monte Carlo Approach To Study Carbonate Dissolution. *J. Phys. Chem. C* **2016**, *120*, 6482−6492.

(33) Rohlfs, R. D.; Fischer, C.; Kurganskaya, I.; Luttge, A. Crystal Dissolution Kinetics Studied by a Combination of Monte Carlo and Voronoi Methods. *Minerals* **2018**, *8*, No. 133.

(34) Kurganskaya, I.; Rohlfs, R. D. Atomistic to Meso-Scale Modeling of Mineral Dissolution: Methods, Challenges and Prospects. *Am. J. Sci.* **2020**, *320*, 1−26.

(35) Zhang, L.; Lüttge, A. Al,Si Order in Albite and Its Effect on Albite Dissolution Processes: A Monte Carlo Study. *Am. Mineral.* **2007**, *92*, 1316−1324.

(36) Meakin, P.; Rosso, K. M. Simple Kinetic Monte Carlo Models for Dissolution Pitting Induced by Crystal Defects. *J. Chem. Phys.* **2008**, *129*, No. 204106.
(37) de Assis, T. A.; Aarão Reis, F. D. A. Dissolution of Minerals with Rough Surfaces. *Geochim. Cosmochim. Acta* **2018**, *228*, 27−41.
(38) Lasaga, A. C.; Blum, A. E. Surface Chemistry, Etch Pits and Mineral-Water Reactions. *Geochim. Cosmochim. Acta* **1986**, *50*, 2363−2379.
(39) Berner, R. A. GEOCARB II: A Revised Model of Atmospheric CO[Sub 2] over Phanerozoic Time. *Am. J. Sci.* **1994**, *294*, No. 56.
(40) Berner, R. A.; Kothavala, Z. Geocarb III: A Revised Model of Atmospheric CO2 over Phanerozoic Time. *Am. J. Sci.* **2001**, *301*, 182−204.
(41) Bouissonnié, A.; Daval, D.; Ackerer, P. Dissolution Anisotropy of Pyroxenes: A Surrogate Model for Steady-State Enstatite Dissolution Resulting from Stochastic Simulations of the Hydrolysis Process. *J. Phys. Chem. C* **2020**, *124*, 13113−13126.
(42) Hugh-Jones, D. A.; Angel, R. J. A Compressional Study of MgSiO3 Orthoenstatite up to 8.5 GPa. *Am. Mineral.* **1994**, *79*, 405−410.
(43) Cailleteau, C.; Angeli, F.; Devreux, F.; Gin, S.; Jestin, J.; Jollivet, P.; Spalla, O. Insight into Silicate-Glass Corrosion Mechanisms. *Nat. Mater.* **2008**, *7*, 978−983.
(44) Devreux, F.; Ledieu, A.; Barboux, P.; Minet, Y. Leaching of Borosilicate Glasses. II. Model and Monte-Carlo Simulations. *J. Non-Cryst. Solids* **2004**, *343*, 13−25.
(45) Hellmann, R.; Cotte, S.; Cadel, E.; Malladi, S.; Karlsson, L. S.; Lozano-Perez, S.; Cabié, M.; Seyeux, A. Nanometre-Scale Evidence for Interfacial Dissolution−Reprecipitation Control of Silicate Glass Corrosion. *Nat. Mater.* **2015**, *14*, 307−311.
(46) Gin, S.; Collin, M.; Jollivet, P.; Fournier, M.; Minet, Y.; Dupuy, L.; Mahadevan, T.; Kerisit, S.; Du, J. Dynamics of Self-Reorganization Explains Passivation of Silicate Glasses. *Nat. Commun.* **2018**, *9*, No. 2169.
(47) Wild, B.; Daval, D.; Guyot, F.; Knauss, K. G.; Pollet-Villard, M.; Imfeld, G. PH-Dependent Control of Feldspar Dissolution Rate by Altered Surface Layers. *Chem. Geol.* **2016**, *442*, 148−159.
(48) Daval, D.; Sissmann, O.; Menguy, N.; Saldi, G. D.; Guyot, F.; Martinez, I.; Corvisier, J.; Garcia, B.; Machouk, I.; Knauss, K. G.; et al. Influence of Amorphous Silica Layer Formation on the Dissolution Rate of Olivine at 90 °C and Elevated PCO(2). *Chem. Geol.* **2011**, *284*, 193−209.
(49) Zhang, L.; Lüttge, A. Morphological Evolution of Dissolving Feldspar Particles with Anisotropic Surface Kinetics and Implications for Dissolution Rate Normalization and Grain Size Dependence: A Kinetic Modeling Study. *Geochim. Cosmochim. Acta* **2009**, *73*, 6757−6770.
(50) Dana, E. S. *The System of Mineralogy*; John Wiley & Sons, Inc.: New York, 1899.
(51) Fischer, C.; Arvidson, R. S.; Lüttge, A. How Predictable Are Dissolution Rates of Crystalline Material? *Geochim. Cosmochim. Acta* **2012**, *98*, 177−185.
(52) Daval, D.; Calvaruso, C.; Guyot, F.; Turpault, M.-P. Time-Dependent Feldspar Dissolution Rates Resulting from Surface Passivation: Experimental Evidence and Geochemical Implications. *Earth Planet. Sci. Lett.* **2018**, *498*, 226−236.
(53) Carrasco, I. S. S.; Aarão Reis, F. D. A. Modeling the Kinetics of Calcite Dissolution in Neutral and Alkaline Solutions. *Geochim. Cosmochim. Acta* **2021**, *292*, 271−284.
(54) Fischer, C.; Kurganskaya, I.; Luttge, A. Inherited Control of Crystal Surface Reactivity. *Appl. Geochem.* **2018**, *91*, 140−148.
(55) Beig, M. S.; Lüttge, A. Albite Dissolution Kinetics as a Function of Distance from Equilibrium: Implications for Natural Feldspar Weathering. *Geochim. Cosmochim. Acta* **2006**, *70*, 1402−1420.
(56) Schott, J.; Brantley, S.; Crerar, D.; Guy, C.; Borcsik, M.; Willaime, C. Dissolution Kinetics of Strained Calcite. *Geochim. Cosmochim. Acta* **1989**, *53*, 373−382.
(57) Xu, J.; Fan, C.; Teng, H. H. Calcite Dissolution Kinetics in View of Gibbs Free Energy, Dislocation Density, and PCO2. *Chem. Geol.* **2012**, *322*−*323*, 11−18.
(58) Teng, H. H. Controls by Saturation State on Etch Pit Formation during Calcite Dissolution. *Geochim. Cosmochim. Acta* **2004**, *68*, 253−262.
(59) Lasaga, A. C. Fundamental Approaches in Describing Mineral Dissolution and Precipitation Rates. In *Chemical Weathering Rates of Silicate Minerals*; White, A. F.; Brantley, S. L., Eds.; Mineralogical Society of America, 1995; Vol. *31*, pp 23−86.
(60) Kossel, W. Zur theorie des kristallwachstums. *Nachr. Ges. Wiss. Goettingen, Math.-Phys. Kl.* **1927**, *1927*, 135−143.
(61) Stranski, I. N. Zur Theorie Des Kristallwachstums. *Z. Phys. Chem.* **1928**, *136U*, 259−278.
(62) Skrotzki, W. Defect Structure and Deformation Mechanisms in Naturally Deformed Hornblende. *Phys. Status Solidi A* **1992**, *131*, 605−624.
(63) Luc, N.; André, N.; Damien, D. Rate-Limiting Reaction of C3S Hydration—A Reply to the Discussion "A New View on the Kinetics of Tricalcium Silicate Hydration" by E. Gartner. *Cem. Concr. Res.* **2018**, *104*, 118−122.
(64) Steefel, C. I.; Maher, K. Fluid-Rock Interaction: A Reactive Transport Approach. *Rev. Mineral. Geochem.* **2009**, *70*, 485−532.
(65) Nicoleau, L.; Bertolim, M. A. Analytical Model for the Alite (C3S) Dissolution Topography. *J. Am. Ceram. Soc.* **2015**, *99*, 773−786.
(66) Robin, V.; Wild, B.; Daval, D.; Pollet-Villard, M.; Nonat, A.; Nicoleau, L. Experimental Study and Numerical Simulation of the Dissolution Anisotropy of Tricalcium Silicate. *Chem. Geol.* **2018**, *497*, 64−73.
(67) Daval, D.; Bernard, S.; Rémusat, L.; Wild, B.; Guyot, F.; Micha, J. S.; Rieutord, F.; Magnin, V.; Fernandez-Martinez, A. Dynamics of Altered Surface Layer Formation on Dissolving Silicates. *Geochim. Cosmochim. Acta* **2017**, *209*, 51−69.
(68) Wild, B.; Daval, D.; Micha, J.-S.; Bourg, I. C.; White, C. E.; Fernandez-Martinez, A. Physical Properties of Interfacial Layers Developed on Weathered Silicates: A Case Study Based on Labradorite Feldspar. *J. Phys. Chem. C* **2019**, *123*, 24520−24532.
(69) Zhang, L.; Lüttge, A. Aluminosilicate Dissolution Kinetics: A General Stochastic Model. *J. Phys. Chem. B* **2008**, *112*, 1736−1742.

https://doi.org/10.1021/acs.jpcc.0c11416
J. Phys. Chem. C XXXX, XXX, XXX−XXX